DEVELOPMENT OF HIGH-THROUGHPUT MICROFLUIDIC IMPEDANCE SPECTROSCOPY PLATFORM FOR ANALYZING MICRODROPLETS IN DROPLET MICROFLUIDIC SYSTEM

A Thesis

by

NEBRAS MOHAMMEDKAMAL A. SOBAHI

Submitted to the Office of Graduate and Professional Studies of
Texas A&M University
in partial fulfillment of the requirements for the degree of

MASTER OF SCIENCE

Chair of Committee,	Arum Han
Committee Members,	Jim X. Ji
	Samuel Palermo
	Vladislav V. Yakovlev
Head of Department,	Chanan Singh

August 2014

Major Subject: Electrical Engineering

ABSTRACT

This thesis presents the development of a high-throughput microfluidic impedance spectroscopy platform for electrically detecting analyzing impedance measurements of non-contact and label free microdroplets. This microfluidic impedance spectroscopy platform gives valuable information of the size and contents of the microdroplets in general and particularly of cells encapsulated within droplets.

Impedance spectroscopy is a common method for analyzing dielectric properties of particles with respect to the stimulating frequency. Microfluidic based impedance spectroscopy can analyze up to micro size particles. However, droplets based microfluidic impedance spectroscopy systems for analyzing cells encapsulated within droplets have been rarely developed.

However, to develop a high-throughput system, a novel sensitive high-throughput droplets based microfluidic impedance spectroscopy platform for analyzing cells encapsulated with droplets at different levels concentrations at throughput of 140 Hz which has not been reported in the literature yet.

The device sensitivity was demonstrated using chlamydomonas reinhardtii cells. Two throughputs (17 and 140 droplets/s) for four level of cells concentrations were discriminating and compared. The maximum deviation in the acquired data for both cases was 6.9%. At 10% difference of cells encapsulated within droplets, the device was capable of discriminating and distinguishing different between the encapsulated microdroplets.

DEDICATION

To my dear Father, Mother, Wife, and Son with great love and appreciation

ACKNOWLEDGEMENTS

I am eternally grateful to my advisor and committee chair Dr. Arum Han, for his excellent guidance, caring, patience, and providing me his time to supervise my research work and study.

Many thanks are extended to examining committee members for their guidance and support for my thesis research. Also, I would like to thanks all group members for their help and experience. I would like to thanks King Abdulaziz University and Saudi Arabian Cultural Mission for their financially support my graduate study.

Finally, many thanks to my father, mother, wife, and all family members who were always encouraging and supporting me with their love and best wishes.

NOMENCLATURE

Au	Gold
IPA	Isopropyl Alcohol
iPSC	Induced Pluripotent Stem Cells
LOC	Lab-on-Chip
LPF	Low Pass Filter
PDMS	Poly (Di-Methyl) Siloxane
Ti	Titanium
µTAS	Micro Total Analysis Systems

TABLE OF CONTENTS

Page

LIST OF FIGURES

Page

LIST OF TABLES

Page

CHAPTER I

INTRODUCTION AND LITERATURE REVIEW

1.1. Introduction

Projected future growth influences how the industries and markets request the researchers and developers to have a robust identification and micro sensible systems for various range of biomedical application. Besides, due to these enormous growth rate in technologies, high-throughput is important to effectively characterize and study the substrate of the biological and biochemical components which have significant information that could accelerate understanding many different subjects. High-throughput screening of culture condition is one of the applications that have been significantly widely developed for different aspects such as label free cells discriminating and identification. High-throughput is significantly beneficial in biological and biochemical application if this type of sensors are sufficiently non-contact, non-invasive, label-free, low cost, and highly sensitive. Therefore, droplet microfluidic-based systems have been developed and employed in broad application such as drug and mutant library screening application. Droplet based systems have been shown its capabilities of cells encapsulation and it can be effectively merged with other droplet for drug screening application using passive or active methods [1].

Thus, there is an uncountable number of methods that have been developed and employed for characterizing different state of matter; however, dielectric impedance spectroscopy gives invaluable information for various biological and biochemical

applications. Hence, this work concentrates on developing a high-throughput microfluidic-based dielectric impedance spectroscopy for characterizing cells concentration in droplets.

1.2. Impedance Spectroscopy

Dielectric impedance spectroscopy is a great tool for measuring the dielectric properties of any interested material by measuring the induced reduced electric field due to the dielectric properties of this material. This electric field cross over from a stimulating electrode to another detecting electrode based on its voltage strength and the medium properties as illustrated in Figure 1.

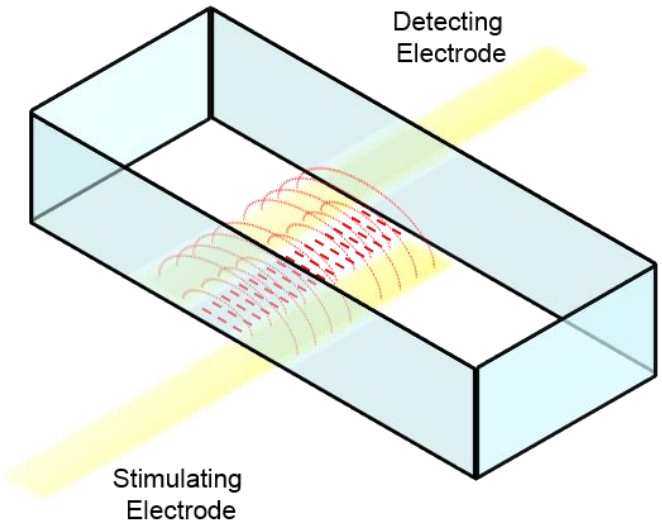

Figure 1: Illustration of electric fields distribution in a medium.

However, one of the main electrical parameter that distort this field is the permittivity of the materials. Permittivity is how much the change of the resistance when the medium influence by an electric field. Permittivity is represented the reduction in the electric field due to the effect of the medium depolarization [2-3]. Besides, the permittivity is formed as complex-valued that describes the phase difference between the applied electric field and the arising one. Therefore, the dielectric spectroscope method is employed to measure the dielectric impedance with respect to spectrum frequency. The dielectric spectroscopy could be used with any materials under test such as solids, liquids, or gases [4-6]. To successfully identified and characterized the impedance measurements, the sample must be fully occupied the detection region. However, this type of technique has been greatly developed to successfully detect and characterize two different medium such as cells or DNA in liquids which has different permittivity comparing to liquid media [7].

The initial concept of impedance come out first from the electric resistance. The electric resistance is the ability of an electric component to resist the electric current that flow through this component. The electric resistance is the relation between the applied voltage and the current that flow through it as defined by Ohm's Law in Eq.1:

$$R = E/I \tag{1}$$

However, this electric resistance measurement could not be applied or used in sophisticated behavior systems to study their electric resistivity due to other electric components that exhibit in a complex form. Therefore, an electric impedance is used

instead of resistance to characterize and measure the ratio of the applied voltage to the AC current that flow through a particular medium. This concept is widely used to characterize the electrochemical properties of several number of mediums such as chemical solutions, cells, and many different biological tissues.

The impedance measurements response of a single-cell have been justified by developing an electric circuit model of a single-cell to interpret the impedance measurements of single-cell in a medium, such as Foster and Schwan's simplified circuit model as illustrated in Figure 2 .

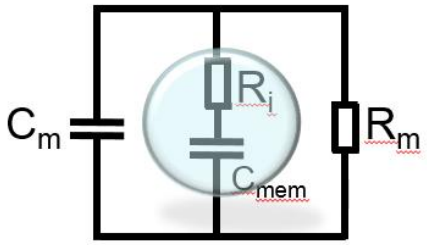

Figure 2: The circuit model of single-cell in a medium.

As shown from this simplified model, the cell is located in suspended media that has two parallel electric components, a resistor R_m and capacitor C_m while the cell was modeled with a series of resistor and capacitor, R_i and C_{mem}. The resistor R_i is equivalent to the resistivity of the cytoplasm of the cell and C_{mem} to the capacitance of the cell membrane. This model has been widely used to agree with the cell impedance measurements [8-11]. This model can clearly interpret how the electric properties of the cell membrane and cytoplasm can be measured. Also, due to capacitance presence effect within the cell and the medium, using an AC signal to therefore result an impedance

measurements that show valuable information of subcellular components of a single-cell. However, the impedance measurement is a function of frequency whereas the amplitude and phase of the cell impedance measurements vary based on the frequency range that is used [12].

1.3. Microfluidic-Based Impedance Spectroscopy

Microfluidics is an abundant tool for purpose of studying the behavior of miniaturized flow at microscale dimensions. Confinement small volume of fluids at this scale can show different behaviors such as laminar flow, surface tension, and electrowetting [13]. Microfluidics is a method that can precisely manipulate fluids by using microscale devices that fabricate using technologies that developed from semiconductor industries. Using these novel devices, enormous influences that enable huge conurbations in many different fields of study, especially biology and medical research [14-18]. Therefore, these miniaturized devices have been widely applied and used for various biological assays due to small sample volume requirements, which results in reducing the total cost of reagents and maximize the outcome invaluable information as consequences from that scale. Microfluidic devices are commonly fabricated using Poly (dimethylsiloxane) (PDMS) material due to, material and surface properties, low cost, and easy fabrication process [19-21].Using microfluidic technologies, cells analysis, discrimination, and sensing have been focused and demonstrated using different methods and technologies such as combing microfluidics with a variety of functional elements that can specifically manipulate and

handle up to single cell. These analysis devices are commonly referred to as micro total analysis systems (μTAS) or lab-on-chip (LOC) [22-24].

Microfluidic-based impedance spectroscopy has been shown great potential due to its capabilities of detecting, sensing, and characterizing particles flow-through fluidic channels at microscale size. Microfluidic-based impedance spectroscopy systems for cell analysis have been developed at two different conditions: trapping and flow-through. Each of these conditions has its advantages and limitations. Impedance analysis of trapped cells is required for an application that need long culture monitoring by trapping the cell between two electrodes and characterize its impedance behavior, for example, capturing single-HeLa cells inside microchannels and performing electrical analysis as a result of impedance measurements [25]. Malleo et al. characterized single cell trapped hydro-dynamically and continuously performed differential impedance analysis [26]. Volume change of captured single cells in a microfluidic device was analyzed by measuring electrical impedance change [27]. A great potential was done by our group to minimize the leakage current besides increasing the trapping sites by fabricating an array of planar electrodes using micro-holes channels for cells trapping and then impedance measurements [28]. The throughput using this method is limited due to long time needed for each analysis for each cell. However, some researchers tried to increase the trapping site to a large number, but this result to increase the system complexity due to an enormous number of multiplexed impedance measurements [29-31]. Beside to the throughput limitation, the cell impedance measurements are affected by many factors such as cell sizes and trapping structure and dimensions.

In contrast, flow-through condition is considered for high-throughput microfluidic-based impedance spectroscopy. Microfluidic based flow-through systems have been broadly used for analyzing various types of cells [32-34]. Many different electrode designs have been reported for more accurate analysis, for example, an impedance of cells flow cytometry was developed using coplanar electrodes. These fabricated electrodes used to focus and electrically detect the flowing cells differentially by acquiring the impedance change [35]. Although they used focusing electrodes, vertically positional variations of cells could result deviation in the recording impedance. Two pair of electrodes were fabricated to be inside the microfluidic channels to reduce the cells position effect by stimulating using the outer pair and detecting using the two inner electrodes. This device was electrically discriminated between normal RBCs and glutaraldehyde-fixed RBCs [36]. Another method was used by fabricating 3D electrodes to have a uniform electric field that cross over the entire height of the channel and to overcome the vertical position issue that is in the planar electrodes [37]. Also, differentiating between living and dead cells using liquid electrodes was demonstrated [38], as well as discriminating between undifferentiated human induced pluripotent stem cells (iPSC) and iPSC derived cardiomyocyte (iPSC) cells [39]. Also, integration impedance detection and electrical sorting for living and dead cells were demonstrated [40]. In addition, high speed single cell analysis using impedance spectroscopy technique was used to differentiate between two different sizes of polystyrene bead particles using maximum length sequence analysis (MLS) [41]. Another microfluidic differential-based impedance cytometer device was developed for discriminating between small polystyrene beads (1μm and 2 μm diameters)

as well as between yeast cells and beads [42]. For further analysis, integration of vision system with differential impedance spectroscopy for direct comparison analysis of yeast cells and polystyrene beads [43], also another integrated system for size, shape, and position determination of cells using impedance measurements were shown [44]. Another integrated complex device was fabricated by combing single-ended and differential electrical electrodes as well as combing trapping sites and flow-through channels to completeness analysis [45].

Many other recent researchers have been focused on discriminating between cells type and size such as using contactless disposable microfluidic impedance cytometer [46], using an external Wheatstone bridge for more sensitivity and differentially measured the electrical impedance response for passing cells, and characterizing of subcellular components of cells using high excitation frequency range up to 500MHz [47-48].

For additional cells analysis, some researchers have been focused on combining electrical and mechanical measurements by continuously aspiring cells through a construction channel and comparing the transit time and impedance amplitude of different cells [49-50]. Another group used a tapered microfluidic channel to maximize the impedance sensitivity [51]. Many other researchers have shown their interests for classifying of cells based on the mechanical microfluidic structure and their electrical impedance response [52].

Most of the previous microfluidics flow-through impedance analysis works, they have tried to have small volume at the detection region to realize high sensitivity. However, this could lead to fabrication limitation and channel clogging issues. To overcome this issue,

a hydrodynamically focusing the suspended particles in electrolyte using high dielectric insulated fluid. Regardless the channel width and by using this focusing technique, discriminating between 1 μm and 2 μm beads as well as Escherichia were demonstrated [53]. A wide microfluidic based differential impedance cytometer for platelet analysis was used by using dielectric sheath to focus the particles within conductive liquid core [54].

1.4. High-Throughput Droplet-Based Microfluidic Impedance Spectroscopy

Droplets-based microfluidic systems have been widely used for cells manipulations, handling, and analysis at high-throughput rates [55-56], such as particles synthesis [57-59] and chemical screening and analysis [60-63]. Using microfluidic device, microdroplets can be generated at different sizes, manipulated such as merging and sorting, and encapsulated with cells for cells and drug effect screening [64-66] at high-throughput of KHz rates could be achieved. However, high-throughput and label-free detection and characterization of cells encapsulated within droplets has been rarely developed, whereas a droplets-based systems for cells electrically sensing had not been developed until EWM, Kemna et al. developed a first droplet-based microfluidic electrical impedance device that can discriminate between viable and nonviable cells within droplets at throughput of 100Hz [67].Using droplets based systems enable of detecting cells within droplets at throughput rate more than 100Hz. Also, for more than single-cell encapsulated within droplet, various concentration levels of cells encapsulated within droplets can be detected and discriminated using impedance spectroscopy.

1.5. Objective and Motivation

The objective of this work is to develop high-throughput droplet-based microfluidic impedance spectroscopy system for discriminating and characterizing the concentration of cells encapsulated in droplets. This research work concentrates on fabricating single-ended planar electrodes and developing label free, non-contact, and highly sensitive discriminating system using the resistivity values of the detecting dielectric impedance change. This work targets broad range of biological and biochemical applications such as cells screening.

CHAPTER II

DEVELOPMENT OF A HIGH-THROUGHPUT DROPLET-BASED MICROFLUIDIC IMPEDANCE SPECTROSCOPY PLATFORM

2.1. Introduction

A high-throughput impedance detection spectroscopy system has been developed and fabricated to detect and discriminate either between different droplets in matter of size or dialectical content properties. The developed device integrates single-ended connection based electrodes which was developed with a gradually reduced in the geometry of the detection region as well as the electrodes dimensions and gaps in order to realize high sensitive sensor that could discriminate and distinguish between different dielectric mediums based on the impedance measurements. To validate the functionality and the sensitivity of the developed system, a preliminary experiment is needed by discriminating based on the impedance measurements among different sizes of empty droplets.

2.2. Design Principle

The single-ended-based connection high-throughput impedance spectroscopy was successfully designed and precisely perfected to be successfully used with droplets diameter size as low as 40µm. The platform is consisting of two main parts: a) the microfluidic channel and b) the sensing electrodes patterned on glass slides as illustrated in Figure 3.

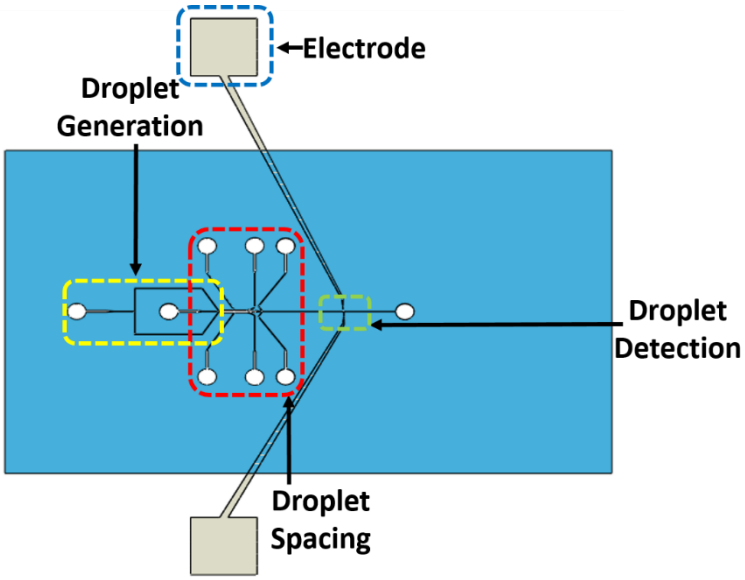

Figure 3: Top view schematic of the developed high-throughput droplet microfluidic-based impedance spectroscopy platform components.

The PDMS microfluidic channel layer involves of three sections: a flow-focusing droplet generation, droplets spacing, and droplets detection sections. Each of these section are explained in further details in the following sections. Micro-electrodes were patterned on (2 X 3 in) glass slide to perform as an electrical stimulating and sensing of the developed platform. The design of each of these parts are explained in more details in the following sections.

2.2.1. Droplets-Based Microfluidics Generation and Spacing

The microdroplets are generated using a flow-focusing droplet generator with three inlet channels. One inlet was split to two continuous-flow channels with 45 µm width are used to precisely control and focus the generated droplets. Another microchannel is added

with 30 µm is used to carry the target fluid such as deionized water to form water droplets in oil. The flow-focusing microfluidics generator has orifice with 50 µm and 60 µm width and height, respectively. The two continuous flow channels are tilted with 120º to help reducing the effect of the back pressure at low flow rates as well as more focusing capability and droplets stability. Also, by using this developed design, diffusion between the carrier oil will reduce and consequently prevent droplets breaking effects at high flow rates for successful high-throughput experiments. The fluids are driven using syringe pumps whereas two syringe pump are used to generate stable micro-sized droplets ranging from 25 µm up 150 µm in diameter as illustrated in Figure 4.

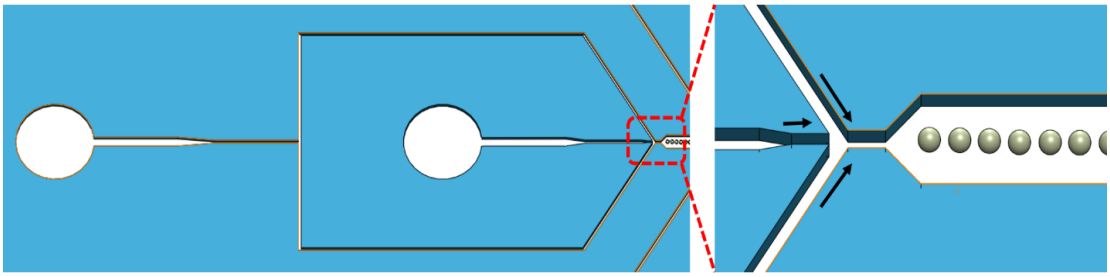

Figure 4: The flow-focusing droplet generation region.

The droplets generator is followed by droplets spacing section which are added to further precisely adjust the spacing between the droplets. Therefore, six carrier oil channels are carefully designed to space between the droplets and regulate again the inserted carrier oil. All of the channel are designed to be tilted for smoother liquid flowing inside the microfluidics channel as depicted in Figure 5.

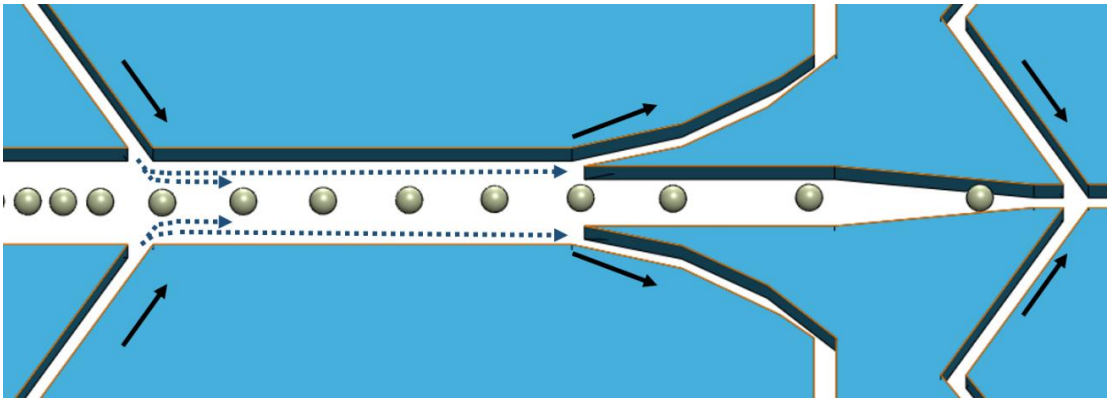

Figure 5: The spacing and focusing region. The left and right inlets pair channels showing how the oil increase the droplets gap and how this oil flow outside this region by using other two channels.

The first carrier oil channels pair is located after the generation section with tendency of 120º and 45µm width. These two channels are tilted for more stability and precisely controlled space between the droplets which can be successfully achieved at very low or high flow rates. Besides, by using this tilting design, less fluctuation at low flow rates due the syringe pump step motion. Also, using this tilted design results more stability of the laminar flow after the droplets generation which help regulating the inserted carrier oil by designing and adding two oil regulating channels that help recycling the carrier oil as well as reducing the oil waste. Moreover, recycling this oil will avoid high shear stress due to the added carrier oil channels that could be break and leaked the microfluidics device. The channels are designed with 55µm width and facing the direction of two inserted carrier oil streams. In the detection channel, another oil carrier channels pair is considered to increase the droplet detection frequency with 45 µm width and 120º tilting

angle. The overall microfluidics height is 60 µm to therefore have detection channel dimensions (60 µm × 60 µm).

2.2.2. Planar Electrodes Detection

Planar detector using gold patterned electrodes are employed to detect and characterize the droplets passing a pair of electrodes. The electrodes were gradually optimized in order to get more sensitivity and accuracy. The gold plated electrodes pattern use to measure the impedance change when any droplet passing by the two electrodes. The width and gap between the electrodes are precisely designed to easily detect and discriminate between different size of droplets after designing and experimentally testing different widths and gaps. The planar electrodes at the bottom of the microfluidic channels as shown in Figure 6.

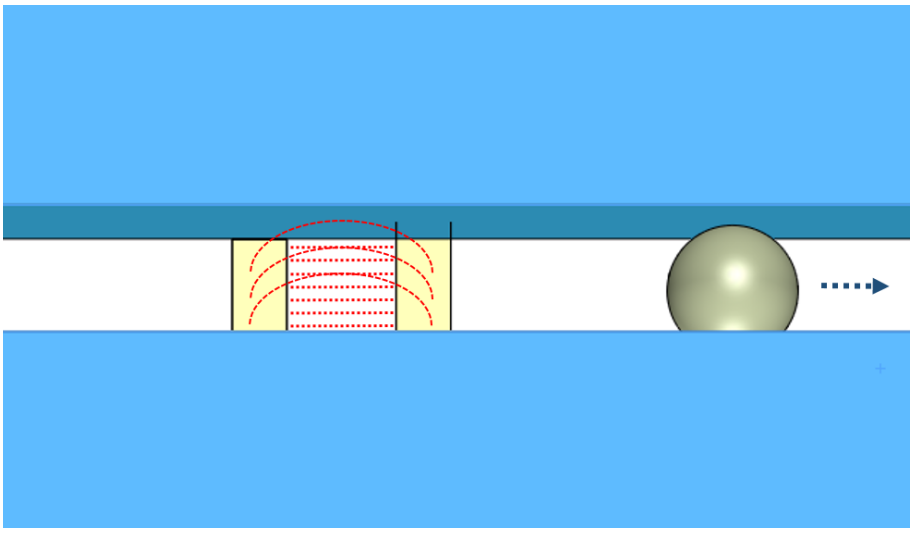

Figure 6: Illustration of droplet passing the sensing region of the developed impedance spectroscopy platform. Also, the illustration represents the electric field lines between the pair of electrodes.

This opposing electrodes design reduce the electric field crosstalk effects that could by using the parallel electrodes. Therefore, the opposing electrodes design is used and precisely aligned inside the microfluidic channel to highly confine the electric field within the detection region; thus, the dielectric measurements are expected to show more sensitivity and accuracy as a result of this accurate design. The gold patterned electrodes with 50µm width and gaps are selected for this conducting research, so the total volume for this detection region is $150 \times 60 \times 60\ \mu m^3$. This planar electrodes design was developed to overcome repeatability and complexity of fabrication techniques to assemble very thin microfluidic channel in between top and bottom patterned electrodes slides. This type of fabrications need more methanol bonding procedures for each electrodes layer for electrodes alignments. The thickness of the glass slide comparing to the microfluidic

channel thickness is massive and significantly generate poor bonding after the second glass slide bonding.

2.3. Devices Fabrication

The droplet-based impedance spectroscopy platform is composed of two layers, a single microfluidic channel layer and a glass slide that comprises of gold patterned electrodes. The single microfluidics channels layer is comprised of three different sections as mentioned before. By soft lithography, the microfluidic channel layer was fabricated using polymimethylsiloxane (PDMS, Sylgard 184, Dow Corning) [68]. Initially, the master mold was fabricated with the standard photolithography techniques starting from piranha cleaning the silicon wafer. Piranha cleaning is a mixture of sulfuric acid and hydrogen peroxide. The hydrogen peroxide must be added to the acid slowly, while that time the temperature of this mixture will be increased; therefore, they should be carefully handled and used. After that, the loaded wafers on the Teflon boat will be immerse after wearing the complete protective clothing in the piranha solution for 10 min, then the boat will be immersed in the preheated DI water at 95^{o}C for 3min or more. After that, the room temperature DI water will be used as the last wet cleaning step to double check of removing any remaining acids on the wafers before touch them for another 3 min or more. During these three immersion steps, the boat should be agitated slowly. After that, the silicon wafers were dried using nitrogen gun to remove any remaining liquid on the wafers. This step must be done to remove any contamination that is on the wafers.

Thereafter, the target height of the microfluidic channel was 60 µm; therefore, to achieve that, the negative photoresist (SU-8 2050) was spin coated at two different speed, 500 rpm for 10 s to uniform the photoresist on the wafer, then 2900 rpm for 30 s to exactly yield 60 µm photoresist thickness. This height was realized after performing and comparing three different speed, 2700, 2800, and 2900 rpm. Then, the wafer was soft baked using a hotplate for 12 hr at 65 ºC and 40 min at 95 ºC. Long soft baking is recommended to generate hard and smooth photoresist layer as well as more adhesion is realized. The wafer was exposed to UV light (Karl Suss MA6 Mask Aligner) using dark field mask at dosage of 200 mJ/cm^2 due to 60 µm photoresist thickness.

A hard baking step was immediately performed to cross link the exposed photoresist by baking the wafers at 65 ºC for 40 min and 95 ºC for 20 min. The dark field mask with negative photoresist makes the non-exposed area be soluble during the development process. Thinner type P is used to remove the non-exposed photoresist and therefore the microfluidic patterned channels were realized by immersing the wafer inside the developer until the non-exposed photoresist completely removed, after that it rinsed with IPA and dried with nitrogen. Thereafter, microfluidic PDMS layer was prepared by mixing pre-polymer and curing agent at weight ratio of 10:1, respectively and degassed using a vacuum chamber for 30 min. then the microfluidic channel layer was casted to form 0.5cm height by mixing 20 mg pre-polymer and 2 mg curing agent. Finally, the PDMS mold was cured for 2 hr at 80 ºC.

The electric electrodes were fabricated using standard photolithography techniques. At first, glass slides were cleaned using the piranha cleaning process. A

uniform of gold (Au) layer was deposited on a glass slide substrates using one of evaporation method of thickness 2000Å. Before that, another layer of titanium (Ti) was deposited as an adhesion layer of thickness 200Å. Gold metal is widely used in biomedical application due to its nontoxic properties and high electrical conductivity comparing to many other metals. Au/Ti films were deposited using E-beam evaporation equipment (Lesker PVD 75 Ebeam Evaporator). Then, a positive photoresist, S1818, was spin coated at 3000 rpm for 30 s onto a gold coated slide, soft baked at 95 ºC for 10min, exposed at 85 mJ/cm^2, hard baked at 110 ºC for 2 min, and developed for 30 s using MF319 to remove the exposed area by using a clear field mask. Thereafter, the glass slides were immersed in gold Au etchant (Type TFA, Transene Company Inc.) to remove the exposed area, then the Ti was etched using Ti etchant (HF:H2O at 1:300). After that, the remaining photoresist was removed using acetone. Finally, the gold patterned glass slides were cleaned using DI water and dried by N_2 gas.

Before bonding the microfluidic channel to the patterned glass slide, a passivation layer is employed to prevent any reaction could happen between the electrodes and samples, also it will avoid droplet hugging on hydrophilic surface that slows down droplet movement. Therefore, 5mg PDMS pre-polymer and 0.5mg curing agent were mixed and degassed, then this mixture was diluted with Hexane with weight ratio 1:1. Hexane solvent is widely used to have very thin PDMS membrane which could generate 10µm or thinner based on a mixing ratio and spin speed and time. Thereafter, the patterned electrode glass slide was spin coated at 4000 rpm for 40 s to generate 10-5 µm membrane thickness and cured at 80 ºC for 2 hr. Finally, the PDMS microfluidic channel casting mold was aligned

and bonded on glass slide after treating the two parts with oxygen plasma chamber (100 mTorr at 100 W) for 1.5 min. The resulted fabricated device as shown in Figure 7. Finally, two SMA connectors were soldered using flux to enhance the soldering efficiency.

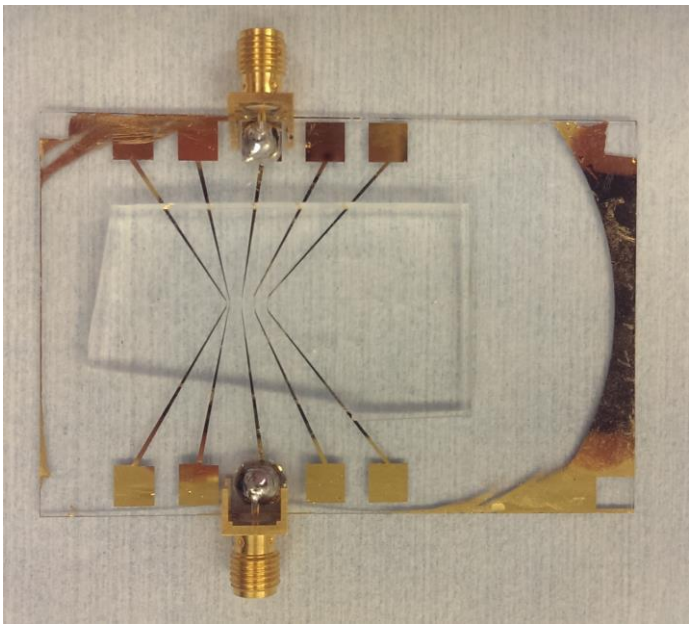

Figure 7: The fabricated microfluidic impedance spectroscopy platform.

2.4. Characterization and Discrimination of Droplets Based on Size

The single-ended impedance spectroscopy platform was developed to discriminate between different percentage levels of concentration of cells encapsulated within droplets, however a preliminary experiment was conducted to show the functionality and the level of sensitivity of the developed platform. Therefore, eight impedance measurements were performed for eight different droplet sizes.

However, initially the stimulating signal should be well-known. Selecting the optimal frequency that could uses depends on many different number of parameters that

significantly affect the impedance measurements. Therefore, the electrical impedance response of the developed system was performed to find the optimal frequency that results a maximum difference between the two impedance measurements for both mediums such as mineral oil and DI water. For this particular experiment, mineral oil as continuous phase and DI water as main phase were used to generate as a result water droplets in oil. Thus, the microfluidic channels were filled and continuously flown all inlet channels with DI water, then all inlet channels were filled and continuously flown by mineral oil. For each liquid phase, the impedance response for the frequency range of 1 KHz to 50 MHz was recorded using an amplitude of 1 V_p. The optimal frequency that results maximum impedance difference between the two experiments was selected.

Thereafter, starting from droplets generation section, the microdroplets were generated using two syringe pumps which were each one was driven at different flow rate. Different stable microdroplets sizes were generated using two different flow rates, whereas the size of the generated droplets is significantly affected by the geometry dimensions of the droplets generation channels. DI water was used as dispersed phase to generate water droplet in oil. Mineral oil is mixed with surfactant (Abil EM90, Evonik) to generated staple size droplets for long term experiment as experimentally tested. The surfactant of 3 % (v/v) was significantly shown more stabilizing in the generated droplet at low flow rates and thereby successfully outcomes at high flow rates. The fluids were driven by syringe pumps. One syringe pump was used to drive the DI water, and two syringe were used another syringe pump to drive the continuous oil phase to generate the droplets. By using two different syringe pumps, different sizes of stable microdroplets

were achieved by adjusting the flow rate from each syringe pump. Another four carrier oil syringes were driven to the microfluidic device using another syringe pump. Due to the use of oil as a surrounding phase, it will prevent the water to wet the PDMS wall inside the microfluidic channels, thus there is no need to coat the microfluidic channels to avoid any water contamination which could decrease electrodes sensitivity. The droplet sizes were analyzed after taking brightfield images with a Zeiss 200M inverted microscope using an HAMAMATSU Digital CMOS Camera ORCA-Flah2.8 C11440 (Carl Zeiss). Different flow rates were employed to generate initially different droplet sizes. Initially, the droplet-based microfluidic impedance spectroscopy platform was characterized using a multi-channel impedance analyzer (HF2IS, Zurich Instruments AG) which was connected to one of the electrode in the platform to supply the sensor with AC volt that generate electric field between the two electrodes within the detection region. This excitation signal is applied to this electrodes to therefore measure the corresponding current response in the second electrode. The acquired current by the opposing electrode was connected to current amplifier (HF2TA, Zurich Instruments AG) to boost the current 10 times or more before it connected back to impedance analyzer (HF2IS). The current amplifier was placed close to the setup to reduce signal losses and any surrounding interference. Also, the Zurich instruments has other options to enhance the acquired signal such as low pass filter (LPF) up to 8^{th} order, so the 8^{th} order LPF was selected which is required after the stage of the demodulation in the Zurich system. The feedback resistor in the Zurich current amplifier was selected to be 100K (V/A) which is recommended to be used due the selected frequency of 550 KHz which is less than 1.5MHz [69]. The main

oil flow rates that in the droplet generation was driven starting from 330 µL/hr to 190 µL/hr. Moreover, the DI water inlet was driven using another syringe pump starting from 20 µL/hr up to 160 µL/hr. Both of these two inlets stepped down/up by 20 µL/hr, respectively to maintain the same number of generated droplets per second. In addition, the other four carrier oil inlets for spacing and focusing were driven using 4 ports syringe pump with 100 µL/hr flow rate. Figure 8 shows the schematic experimental setup diagram of the high-throughput microfluidic impedance spectroscopy platform.

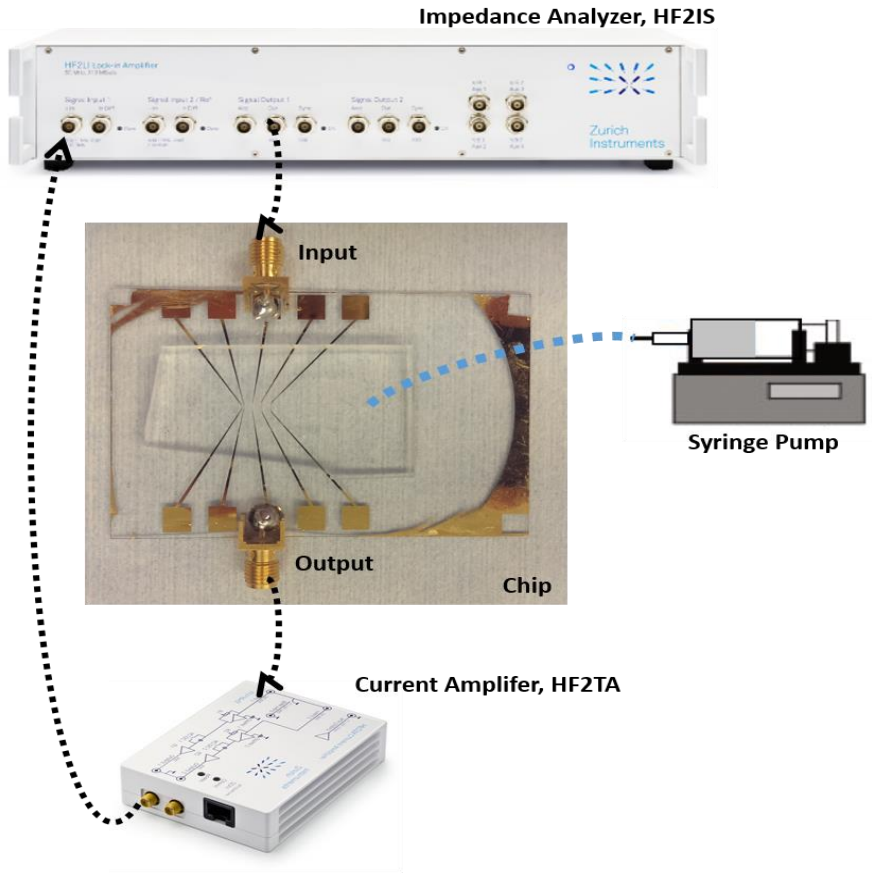

Figure 8: Schematic diagram of the experimental set-up.

2.5. Results and Discussions

The average generated droplets was 95 droplets/s as a result of 8 different experiments. Furthermore, the resulted generated droplets diameters were 53.26, 63.04, 66.30, 71.74, 75, 79.35, 84, and 91.30 µm. Each droplets size was successfully discriminated using the developed single-ended high-throughput impedance platform after selecting the optimal frequency that maximizes the amplitude of the impedance difference between the two liquids. As shown in Figure 9, the optimal frequency that maximizes the amplitude of the impedance difference between the two liquid phases was 550 KHz. Also, at this frequency, the reduced form of the stimulated sinusoidal wave signal could be detected. However, there were other frequency ranges that give higher amplitude impedance difference but the detected signal could not recovered the stimulated signal these ranges. Therefore, 550 KHz was selected as the optimal frequency for this particular device and experiment.

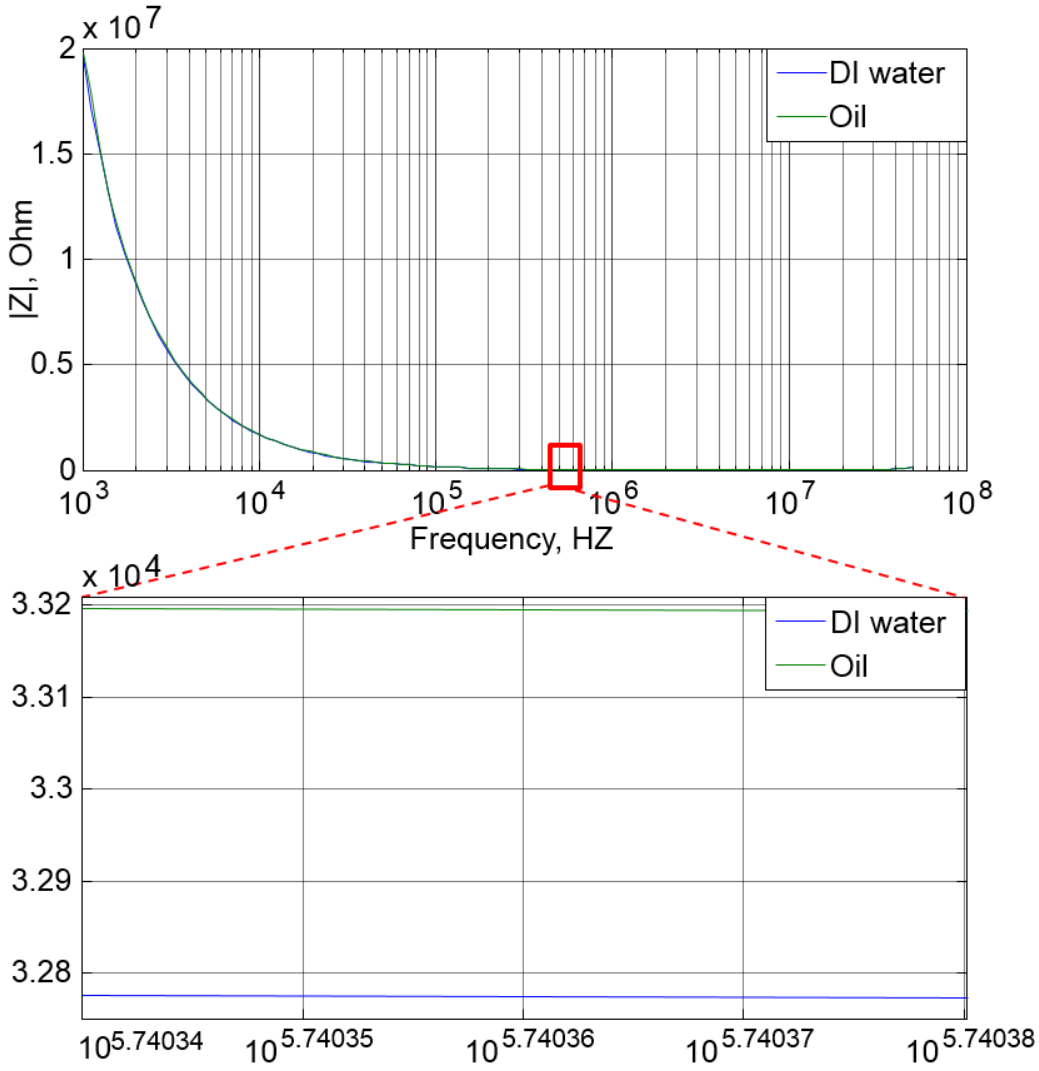

Figure 9: The amplitude impedance response measurement of the developed device versus frequency.

Figure 10 shows the measured droplets diameter when the ratio of DI water flow rate to mineral oil flow rate increased. These measurements were performed using the inverted microscope as shown side by side in Figure 11.

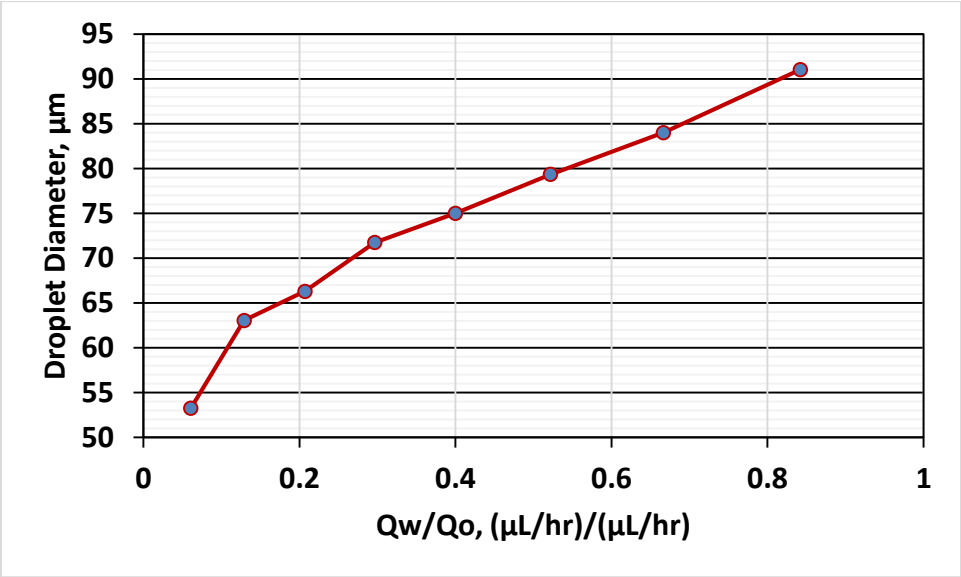

Figure 10: Measured the droplet diameter versus the ratio of DI water flow rate (Q_w) to mineral oil flow rate (Q_o) in µL/hr.

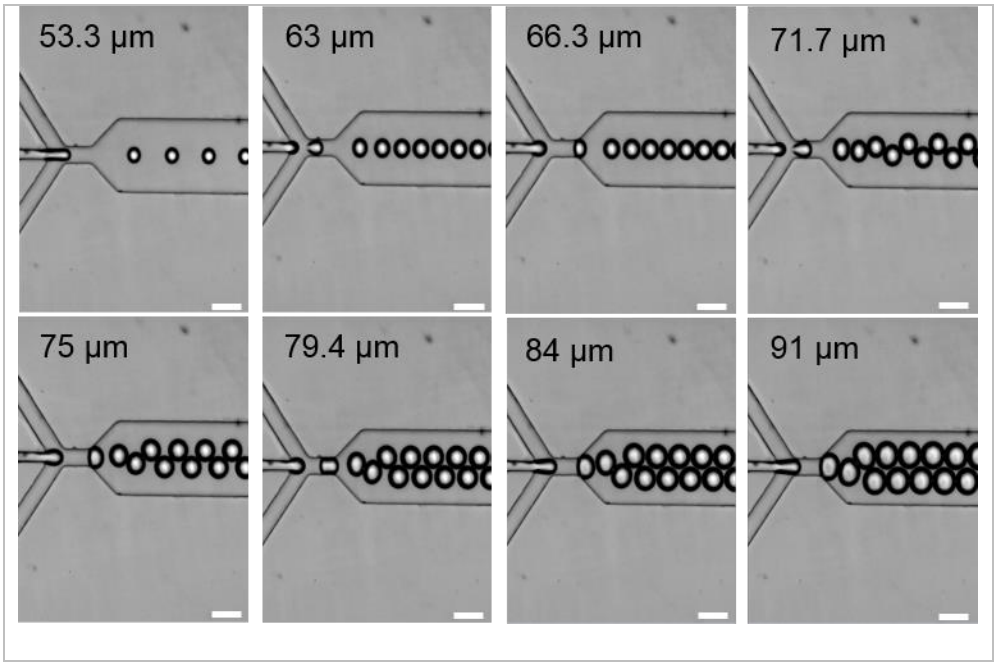

Figure 11: The produced droplets at different ratio of Qw/Qo. The scale bar is 100 µm.

The impedance measurements have been successfully recorded using the developed device by showing increasing in the average impedance change when the droplet sizes were increased as represented in Table 1.

Table 1: The impedance measurement results of discriminating droplets-based sizes.

Experiment No.	water inlet (µL/hr)	oil inlet (µL/hr)	Mean (Ω)	SD (Ω)	RSD (%)	Droplet Diameter (µm)
1	20	330	38.19	7.56	19.80	53.26
2	40	310	69.70	8.65	12.41	63.04
3	60	290	81.05	6.85	8.45	66.30
4	80	270	93.11	10.66	11.45	71.74
5	100	250	99.15	8.55	8.62	75.00
6	120	230	103.30	6.75	6.53	79.35
7	140	210	109.54	8.23	7.51	84.00
8	160	190	128.33	15.76	8.63	91.03

In this table, the resulted average impedance are clearly shown their raise when the droplet diameter is increase. For more accurate results, the real impedance change was utilized after the average the acquired data was achieved. Likewise, the standard deviation (SD) are the relative standard deviations of these peaks were calculated.

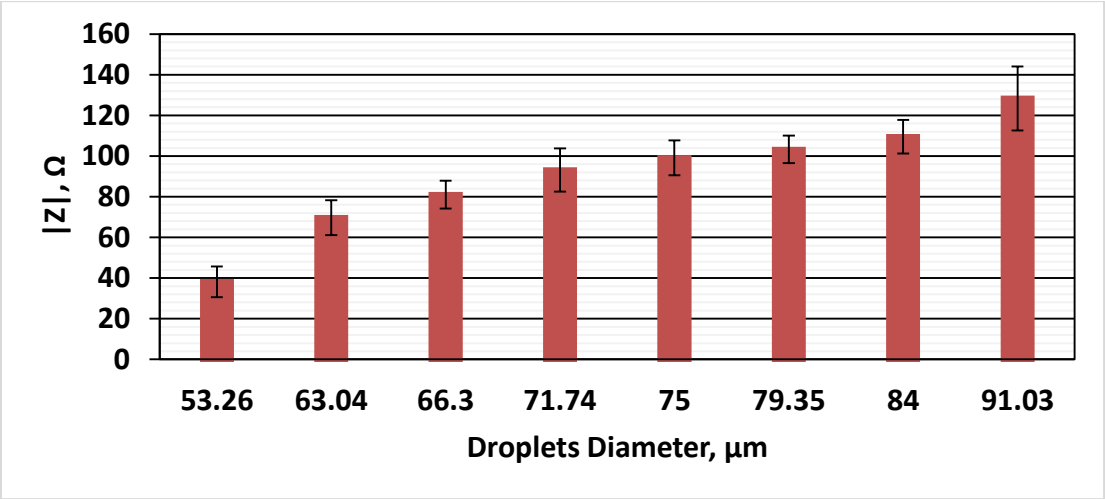

Figure 12: The real average impedance change for eight different droplet sizes. Sample size n=10.

Figure 12 shows the real average impedance change and the standard deviation for the eight experiments. The experiments results shown negative peaks due to more conductivity or less dielectric properties in the DI water droplets comparing to the baseline, the carrier oil, when these droplets pass the sensing region; consequently, the intensity of the electric fields between within the sensing region were increased due to presence of more conductivity media which results reducing in the total real impedance value between the two electrodes as shown in Figure 13. However, the phase difference measurements were ignored due to their poor results; in contrast, the amplitude impedance values were sufficient to clearly distinguish and characterize the droplets size.

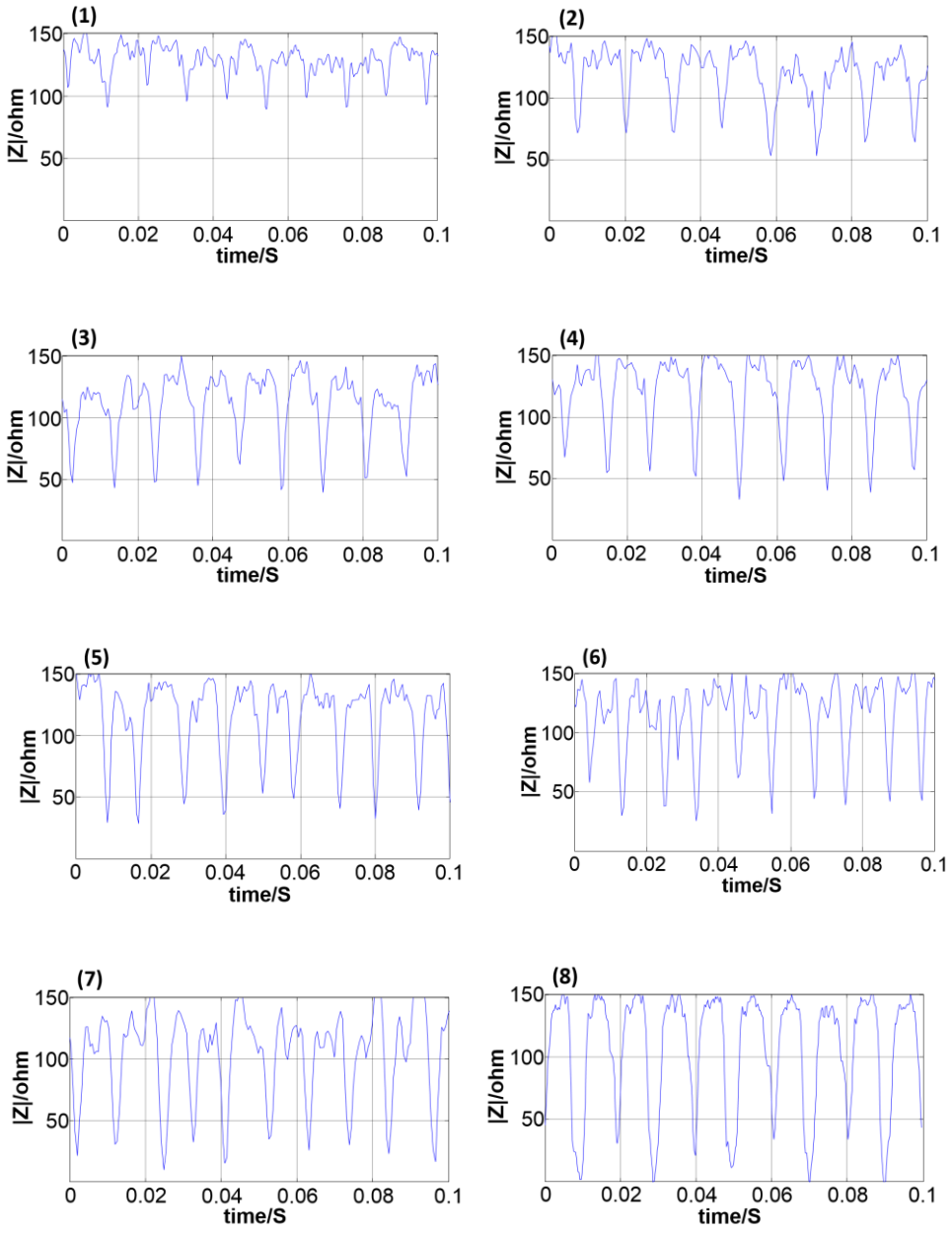

Figure 13: Eight different experiments for size discriminating of droplets using single – ended impedance spectroscopy platform.

The fluctuations that in both the baseline and negative peaks are due to single-ended measurement which could acquire more noise from the surrounding equipment,

power cables, movement in the setup, and syringe pumps motor steps. However, the maximum relative standard deviation in these experiments was in the smallest droplet size experiment, 53.26 µm diameter. As mentioned before, the electrodes were designed to be planar and the width and height of the microfluidic channel at the detection region are 60 µm which is less than the smallest droplet diameter. On the other hand, the intensity of the electric fields gradually decreased in the vertical position and result a variation in the magnitude of the electric impedance signal due to vertically positional droplet dependent. However, at this deviation of ±19.8%, it was still represented small deviation from the average measured impedance change using this single-ended impedance measurements.

2.6. Conclusions

High-throughput droplets-based microfluidic impedance spectroscopy system has been successfully developed using single-ended connection microelectrodes. This device has shown as a preliminary experiments to validate the system performance and accuracy its success in discriminating up to 3.26 µm diameter difference between the droplet diameter sizes. This device can be used to differentiate among different level of cells concentration encapsulated within droplets using only the amplitude values of the impedance measurements due its sufficiently.

CHAPTER III

HIGH-THROUGHPUT DETECTION AND CHARACTERIZATION OF CELLS CONCENTRATION WITHIN DROPLETS

3.1. Cells Preparation

The system was experimentally tested using chlamydomonas reinhardtii cells. They were used to discriminate and distinguish the concentration differences using the developed high-throughput microfluidic impedance spectroscopy platform. C. reinhardtii cells were cultured using TAP culture medium. The cells were filtered using 40 µm diameter filter-cap to remove any cells contaminations. The cells culture were sustained at ambient conditions. The cells were conducted to 12 hour light as well as 12 hour dark periods for 5 days [70]. Thereafter, different percentages of this culture were suspended with 1mL of fresh TAP medium.

3.2. Experimental

Discriminating of C. reinhardtii cells concentrations was performed using single ended-high-throughput impedance spectroscopy platform. Initially, due to using different liquid as dispersed phase, the culture media, the optimal frequency need to be defined. Therefore, the platform was continuous-flowed using oil in all inlet channels at total flow rate that is equal to the real experiment. Also, the dispersed channel was used with oil instead DI water or culture media. The continuous-flow, the dispersed, and the spacing and focusing channels flow rates were 600, 100, and 50 µL h-1, respectively. A frequency

sweep using the Zurich instrument (HF2IS) was performed for the developed platform to characterize the optimal frequency that gives maximum impedance measurement. Again, the experiment was repeated using culture media.

Then, an empty culture media droplets were generated, acquired and characterized their impedance changes to be used as reference value. C. reinhardtii cells were suspended and encapsulated in droplets at various level of concentrations of 10, 20, 30, and 40 % (v/v) of cells inside droplets. For each concentration, the cells were suspended in 1mL of culture media as mentioned before. The developed platform was connected and supplied with 1 AC volt signal of 550 KHz which was connected to stimulation electrode. The electrodes pair measures any droplets passing between the two electrodes when the intensity of the total electrical fields drop or increase due to another dielectric or conductivity media passing within this sensing region. However, in this conducted research, the continuous phase was mineral oil and the generated droplets were culture media with or without cells. The acquired current was low due to poor conductivity media between the two electrodes because the mineral oil was used as a droplets carrier. Therefore, the Zurich current amplifier (HF2TA) was connected to amplify the tiny output current before it was connect back to the impedance analyzer. The amplifier feedback resistor was sit to 100 KΩ. The acquired signal was sampled at a rate of 1.8 KS/s. Mineral oil was used as carrier fluid for the encapsulated droplets and stabilized with surfactant of 3% (v/v). The culture media and oil flow rates were controlled separately using two different syringe pumps to generate stable rate and size of droplets where the two flow rates were 100µL h-1 and 600µL h-1, respectively. Also, the spacing and focusing

channels were driven using another syringe pump 50 µL h-1 for each syringe. The developed impedance spectroscopy platform was mounted and visually observed on the stage of the inverted microscope (Carl Zeiss). The experiments were conducted at room temperature. The further analysis was performed using Matlab®. Figure 14 illustrate the cells suspensions, encapsulation within droplets, spacing and focusing, and finally impedance detection.

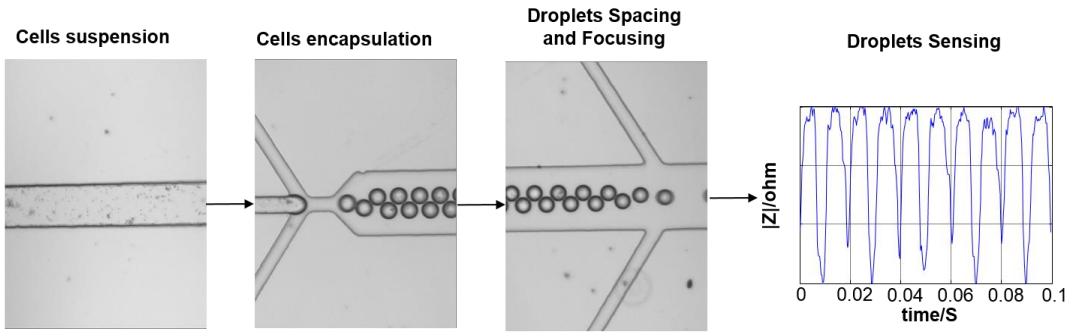

Figure 14: Illustration of cells suspension, encapsulation, spacing and focusing, and detection.

3.3. Results and Discussion

3.3.1. Frequency Sweep

The mineral oil and culture media were separately flown in all inlets and characterized their electrical complex impedance values. Figure 15 shows the impedance response of frequency sweep measurements by sweeping the frequency from 1 kHz to 50MHz. From the resulted amplitude impedance response, there are several ranges of low frequencies give high impedance difference between both liquids. However, the selected voltage for this experiment was 1V as the conducted preliminary experiment. As a result of that, the intensity of the electrical fields between the two electrodes was very low. Therefore, the detected AC signal which is formed in sine wave signal should be detected by the impedance analyzer (HF2IS) as this equipment provide this type of signal. Nevertheless, the frequency that was selected for this experiments was 550 KHz. At this frequency, the amplitude impedance difference was 420 Ω whereas the detected signal was clearly shown small noisy AC signal but it was still could be easily recovered during the demodulation process in Zurich instrument (HF2IS).

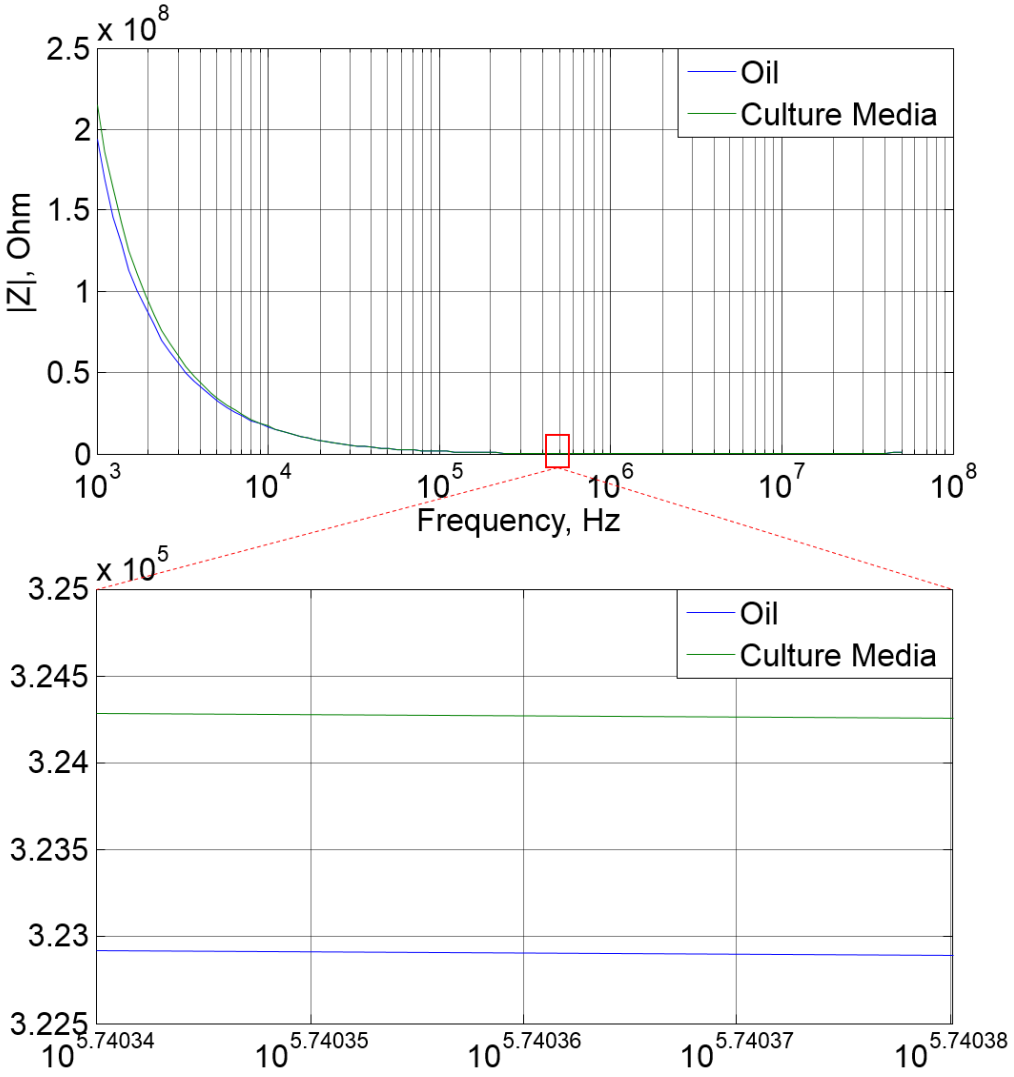

Figure 15: The amplitude impedance response measurement of the developed device versus frequency using culture media and oil.

3.3.2. Low-throughput

At low throughput electrical impedance detection and discrimination for cells concentration encapsulated in droplets, the results show that the impedance values, real values, increased by increasing the cells concentration within droplets.

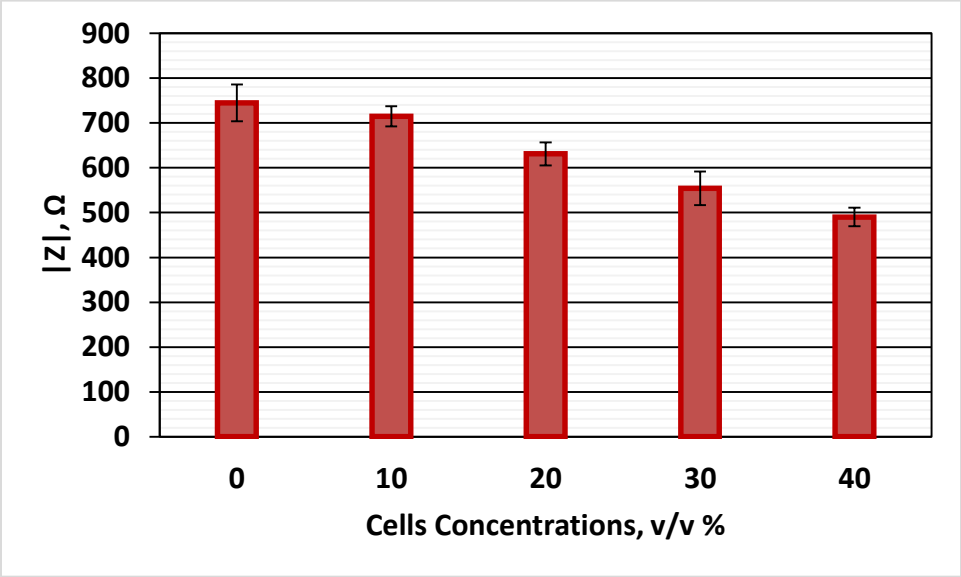

Figure 16: The low-throughput average impedance change of four concentration of cells encapsulated within droplets. Sample size is n=17.

Table 2: The low-throughput result of the impedance measurements.

Cell Concentration (v/v% in 1mL)	Mean (Ω)	STD (Ω)	STD (%)
0	744.84	41.11	5.52
10	715.10	22.63	3.17
20	631.01	25.65	4.07
30	554.32	37.43	6.75
40	490.25	20.68	4.22

Figure 16 illustrates real part of the average impedance changes at four gradually concentrations (10, 20, 30, and 40 % (v/v)) of cells encapsulated in droplets. For further analysis, Table 2 demonstrates the mean and standard deviation at each level of cells concentration whereas at level 0%, droplets without cells was 744.84±41.11 Ω by 5.52% deviation in the mean impedance as shown in Figure 17.

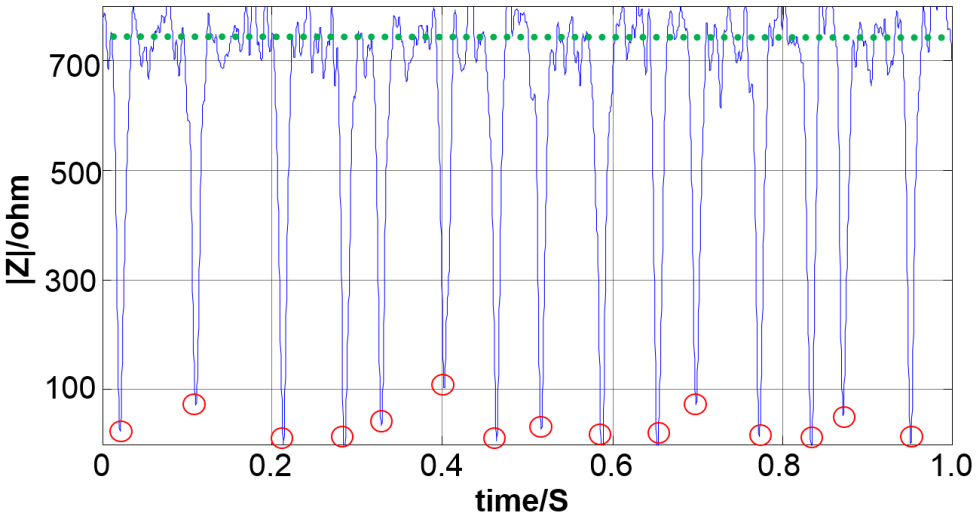

Figure 17: The detected amplitude impedance change of empty droplets.

Figure 18 depicts the amplitude impedance drop when the droplets passing the sensing region. It shows clearly from Figure 18(A-D) how the negative peaks were decreased when the encapsulated cells increased by 10% at each experiment. However, due to difficulty to achieve 100% controlling the number of cells encapsulated within

droplets, there were fluctuations in the base line, the green line as well as the negative peaks impedance values as shown Figure 18(A-D).

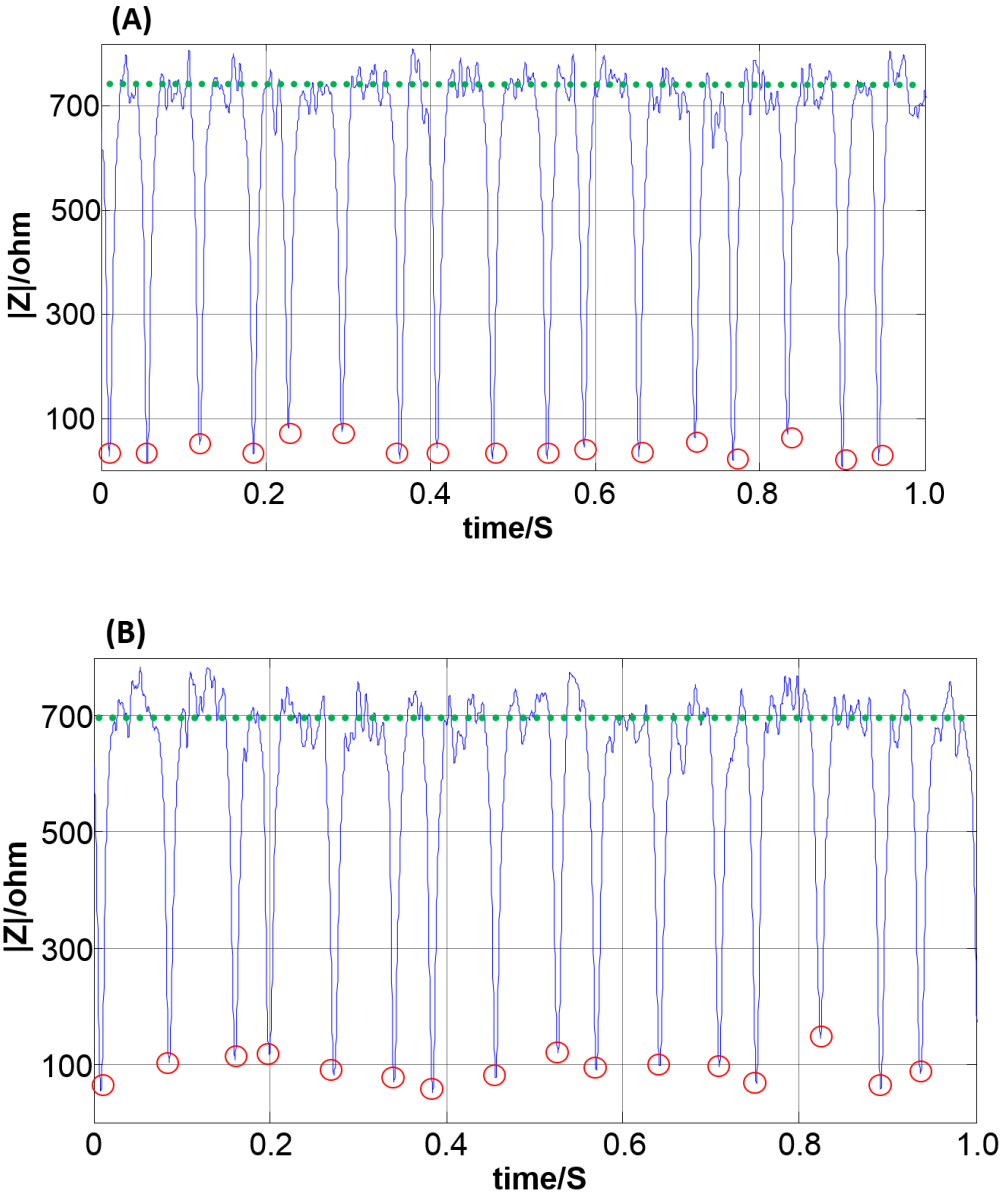

Figure 18: The low-throughput detected amplitude impedance change of four different concentrations of cells within droplets. Four concentrations (10, 20, 30, and 40% (v/v)), respectively from A-D.

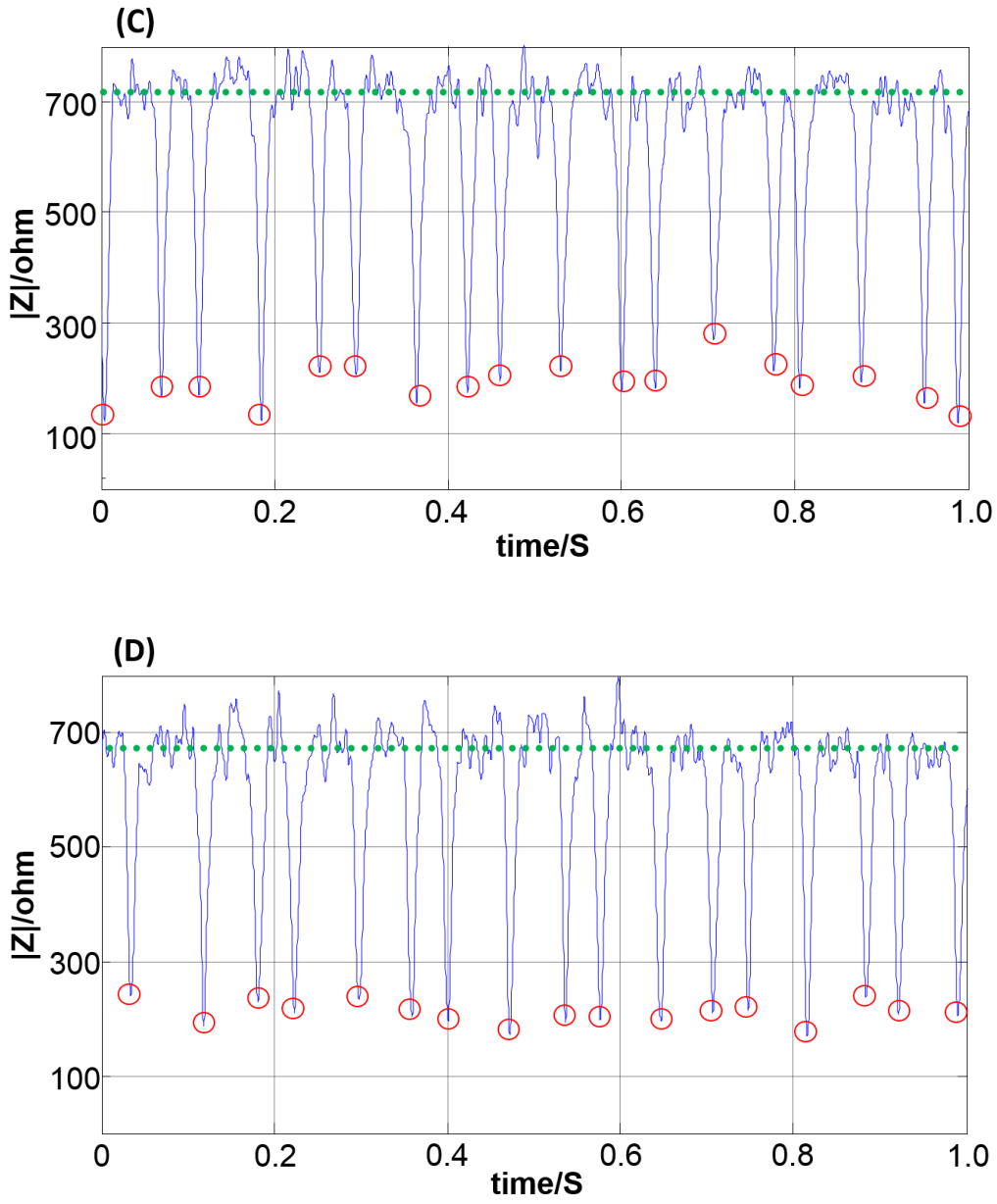

Figure 18: Continued.

However, a successfully achievements have been shown using single-ended impedance spectroscopy platform for detecting and discriminating of an average rate of 17 droplets/s. At this detection rate, the maximum relative standard deviation was 6.75%.

Also, from the average impedance change results, the average drop in the average impedance was 63.65Ω for each 10% increment in the cells concentration within fixed size droplets of 58.7µm diameter.

3.3.3. High-throughput

A high-throughput impedance discriminating for microdroplets encapsulated with four different level of C. reinhardtii cells concentrations have been proficiently achieved. A throughput of 140 Hz was realized. As this high-throughput was obtained in this work and have not been reported in the literature before for discriminating cells within droplets using impedance spectroscopy method, it efficiently shows an average drop in the total real impedance values by 59.44 Ω for each increment in the total cells encapsulated in droplets as shown in Figure 19. The electrical impedance measurements were successfully performed for droplets without and with cells at four different concentrations (10, 20, 30, and 40%) of cells suspended in culture media where the mean and standard deviation of negative peaks were analyzed as tabulated in Table 3 for sample size of n =28.

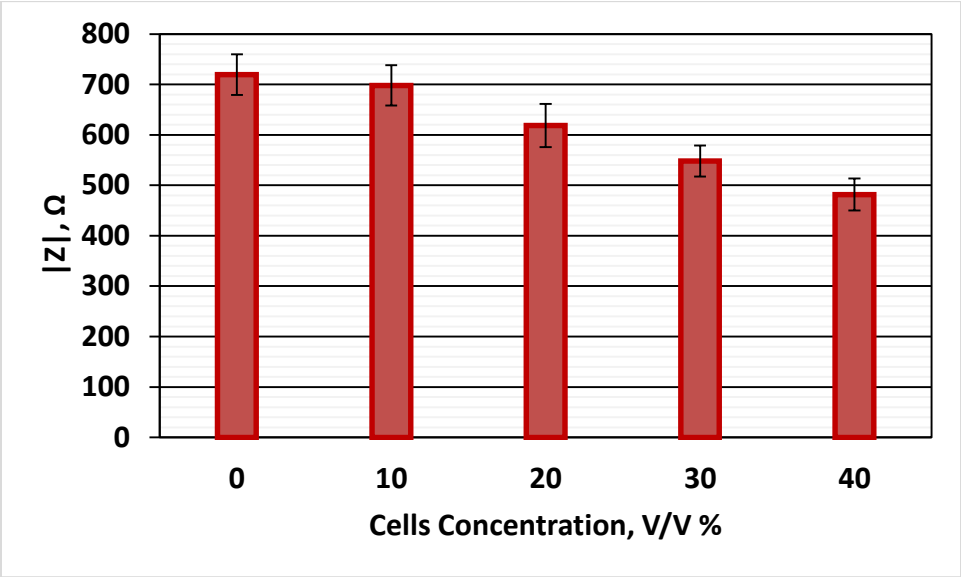

Figure 19: The low-throughput average impedance change of four concentration of cells encapsulated within droplets. Sample size is n=28.

Table 3: The high-throughput results of the impedance measurements.

Cell Concentration (v/v% in 1mL)	Mean (Ω)	STD (Ω)	STD (%)
0	719.48	40.09	5.57
10	698.20	39.77	5.70
20	618.70	42.66	6.90
30	547.97	30.9	5.64
40	481.72	31.83	6.61

In addition, the maximum deviation in the acquired data at high-throughput was 6.9% deviation of an average impedance of 618.7Ω at 20% (v/v) of Chlamy cells encapsulated in droplets.

Figure 20 shows the analyzed negative peaks of the amplitude impedance changes for empty droplets, also for cells encapsulated in droplets at the four concentrations as shown in Figure 21(A-D) were successfully shown how their total impedance changes

decrease by increasing the suspended cells by 10% of each experiment. From Figure 20, it represents the impedance change when empty droplets passing the pair of electrodes where the average impedance change was 719.48±40.09 Ω.

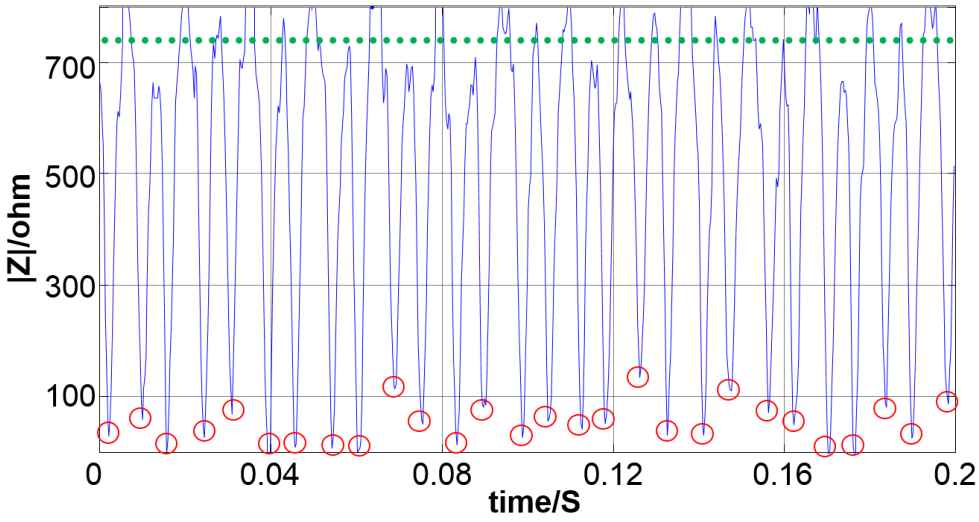

Figure 20: Real part of impedance change for droplet passing between single-ended planar electrodes at rate of 28 Hz for an empty droplets. Sample size n=28.

However, for the cells encapsulated in droplets at cells concentrations of 10, 20, 30, and 40%, the average impedance changes were 698.2, 618.7, 547.97 and 481.72 Ω, respectively. A successfully significant drop in the conductivity were utilized as shown in Figure 21(A-D) in compared to Figure 20 (droplets without cells). When the cells concentration increased inside the droplets, the dielectric particles were increased which results decreasing in the average impedance change values. However, there was a fluctuation in the acquired signals and that could be as a result of the position of cells

inside the droplets. Besides, the measurements setup was performed using single-ended connection whereas any signal fluctuation due to the surrounded noise which could results a drift in the acquired signals. However, the highest deviation in the average impedance changes values in compared to the previous experiments of 17 droplets/s was 6.9% at this high-throughput.

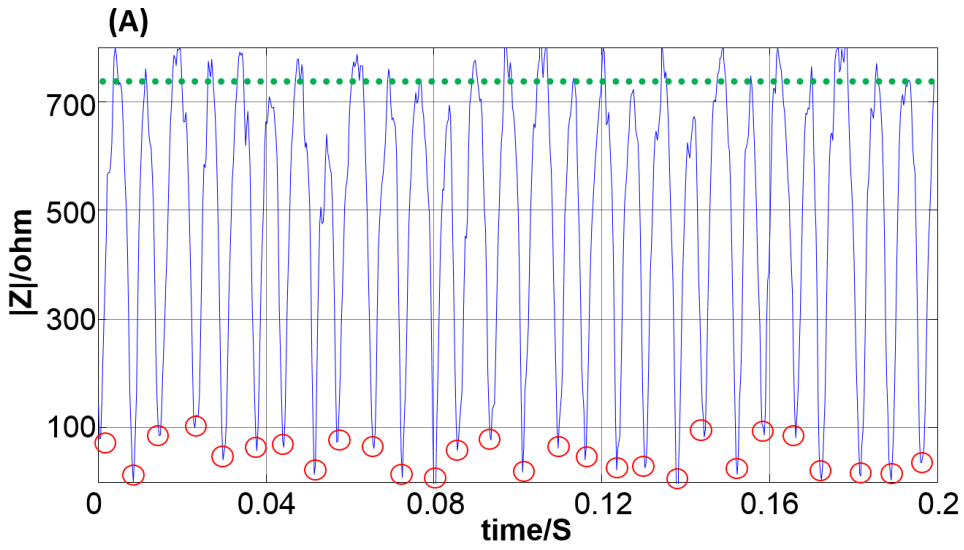

Figure 21: The high-throughput detected amplitude impedance change of four different concentrations of cells within droplets. Four concentrations (10, 20, 30, and 40% (v/v)), respectively from A-D.

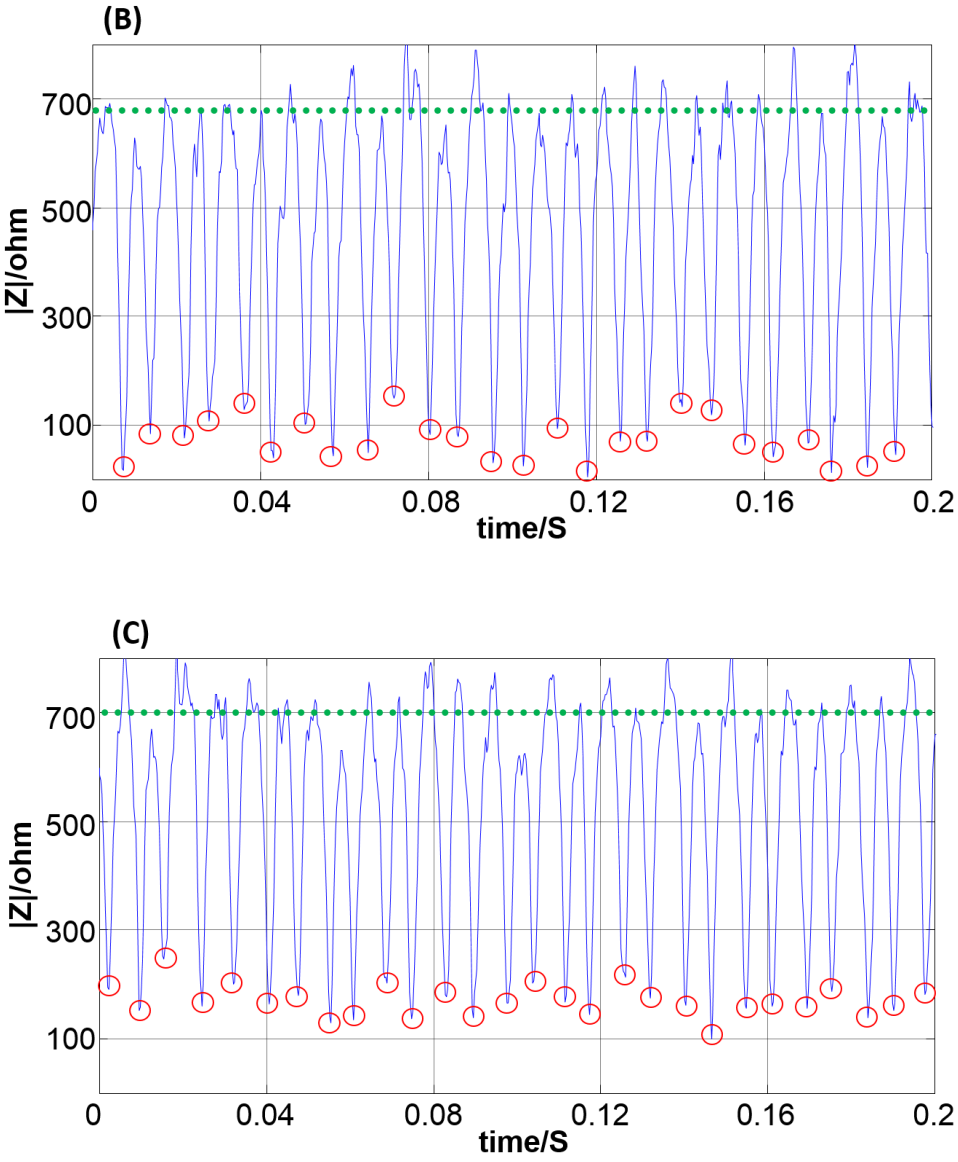

Figure 21: Continued.

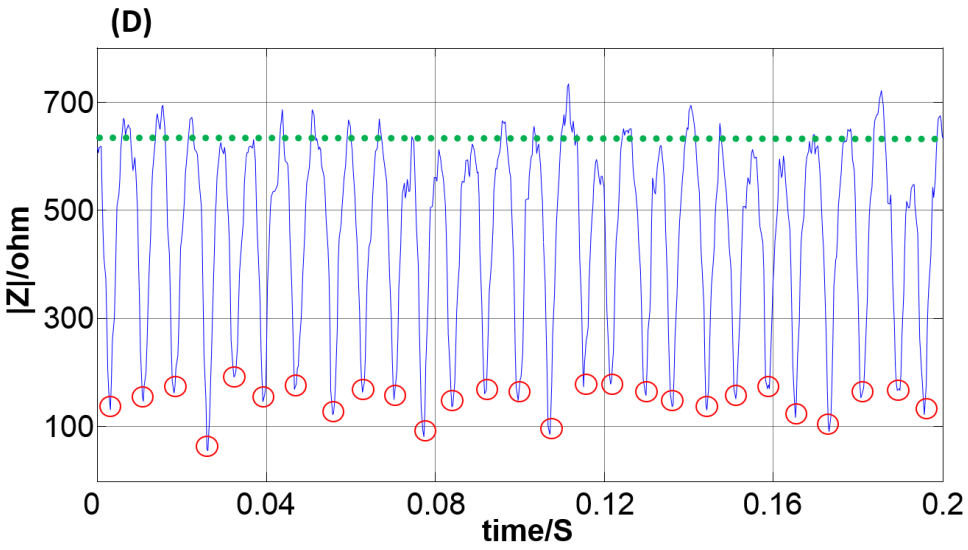

Figure 21: Continued.

3.3.4. Device Repeatability

Run-to-run repeatability of single-ended-based impedance spectroscopy platform was performed by comparing the two different throughput experiments. The impedance change for throughputs of 17 and 140 droplets/s were compared to show the total impedance change difference for both cases and how much difference between them. Figure 22 shows a comparison between these two throughputs which compare the two throughput side by side for 5 different concentrations starting from the empty droplets.

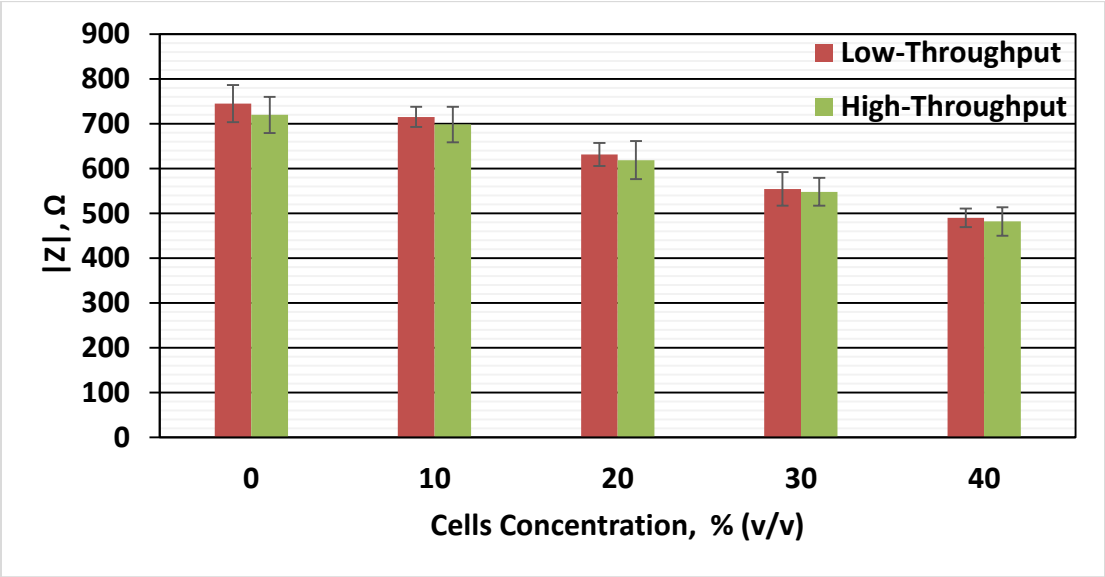

Figure 22: Run-to-run comparison of the repeatability for two different throughput experiments. The sample size of the low and high-throughput were n=17 and 28.

Also, a cross-correlation between the two real impedance averages of at these levels of concentration was successfully achieved by 0.999. Figure 23 shows the normalized real impedance values of both throughputs and how the two throughputs were similar.

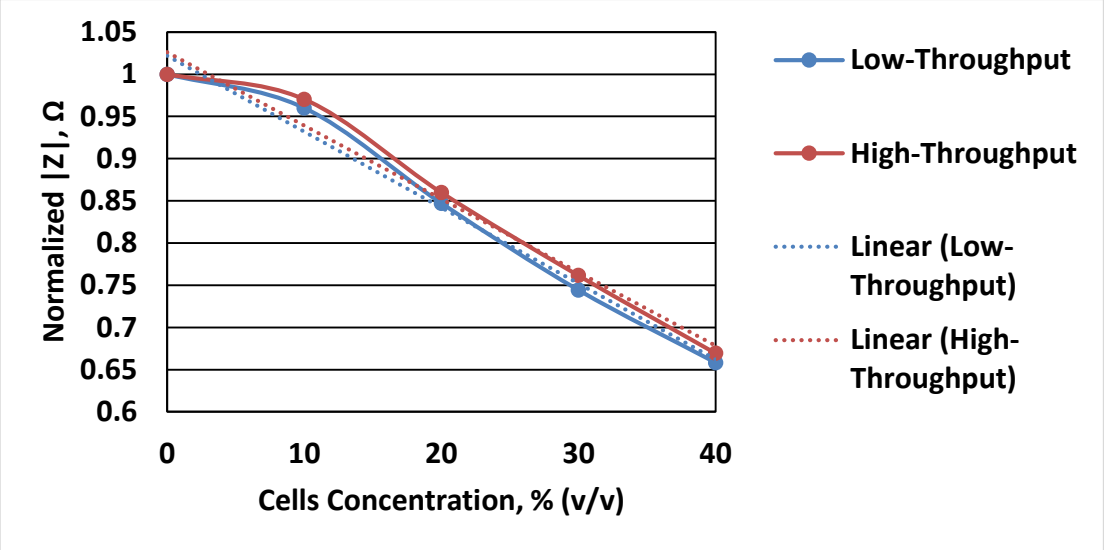

Figure 23: The normalized impedance measurements of both throughputs (17 and 140 Hz) versus the cells concentrations.

3.4. Conclusion

The developed device was used to perform discriminating of cells concentration encapsulated within droplets at two different throughputs. The results from these experiments show how this developed device can use only the sufficient resistivity values of the impedance measurements to differentiate among 4 different cells concentration in compared to the reference result of the empty droplets.

CHAPTER IV

CONCLUSION AND FUTURE WORK

4.1. Conclusion

In this thesis, we have developed a highly sensitive high-throughput droplet-based microfluidic impedance spectroscopy system for characterizing cells concentration within droplets. This high-throughput droplets detection impedance-based device was successfully achieved 140 Hz detection rate which has not been reported in the literatures yet for the cells encapsulated within droplets.

High-throughput droplet microfluidic based impedance spectroscopy platform for cells characterization and discrimination of cells encapsulated in droplets have been successfully developed. Besides, single-ended connection planar microelectrodes were used and fabricated in this developed system. Also, the geometry has been designed and optimized to enhance the sensitivity and accuracy of this device. To overcome the throughput limitations, oil regulation channels have been added which were used not only to shear stress of the high oil flow rate but also to increase the total flow rate and spacing and focusing the droplets.

With this novel device, high-throughput cells encapsulation within droplets and impedance spectroscopy detection using non-contact and label free has been demonstrated. Using C. reinhardtii cells, two throughputs (17 and 140 droplets/s) have been compared and discriminated among four different cells concentrations encapsulated with in culture media droplets. For each of these two throughput, 10% cells concentration

differences can be easily detected and classified by at least 21.28 Ω average resistivity change of the recorded impedance measurements at throughput of 140 Hz. Although the phase difference in all experiments were ignored due to poor results, the amplitude values of the impedance measurements were clearly sufficient to detect and discriminate among different levels of concentrations of cells encapsulated within microdroplets.

Overall, a high-throughput droplets based microfluidic impedance spectroscopy device was developed to discriminate and differentiate between different dielectric medium and particularly among different cells concentrations within droplets.

4.2. Future Works

4.2.1. Differential-Based Impedance Spectroscopy Platform

Design Principle and Set-up

Differential droplet-based microfluidic impedance spectroscopy device has been preliminary developed to reduce the detected noise as well as improve the device performance by characterizing the phase measurements which it will give more valuable information of not only the microdroplets content but also the encapsulated cells.

Differential-based connection impedance spectroscopy platform contains of two different layers, the first layer is a single layer of PDMS microfluidic channel that involves of flow-focusing droplet generator, main detection channel, and the sorting (more details in the next section) as shown in Figure 24.

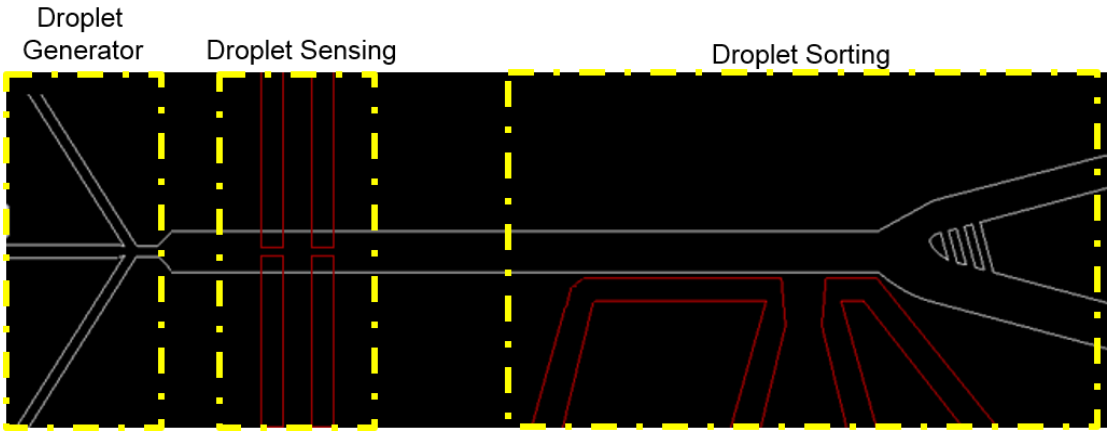

Figure 24: The schematic of the proposed the high-throughput droplet based microfluidic impedance spectroscopy device.

One inlet was designed to carry the carrier fluid after splitting this inlet to two continuous-flow channels with 60 µm width which are used to precisely control and focus the generated droplets. The target liquid that needs to be formulated in droplets such as deionized water is flow throw another microfluidic channel of 60 µm width. The generated droplets are flown inside the main microfluidic channel with 250 µm width. Different pair of differential electrodes were patterned on glass slides of 40µm gap distance between the stimulating and detecting electrodes. For the differential-based connection, another pair of electrodes is located from the first electrodes in a distance of 400µm to be successfully reduced any cross-talk between the two pair of electrodes as well as a reference electrodes when the droplets passing either between the first pair of the second pair. This differential connection was used to prevent any acquiring noise during the impedance measurements. The distance between the generated droplets should be carefully considered due to cancellation possibility in case of two droplets are located between the first and second

pair of electrodes; therefore, the driven two liquids were precisely controlled using two syringe pumps.

Characterization of Droplets based on Frequency

The differential-based impedance spectroscopy platform was preliminary tested to show the effect of the selected stimulating frequencies. The permittivity of any material is formed as a complex-values whereas the dielectric spectroscope method is employed to measure the dielectric impedance with respect to spectrum frequency. Therefore, the generated microdroplets using the differential-based impedance spectroscopy platform was used to show the effect of gradually increasing the stimulating frequency using 15 different frequencies starting from 100 kHz to 20 MHz. This experiments show how the real and phase of the acquired impedance measurements using differential-based connection affected by increasing the excitation frequency.

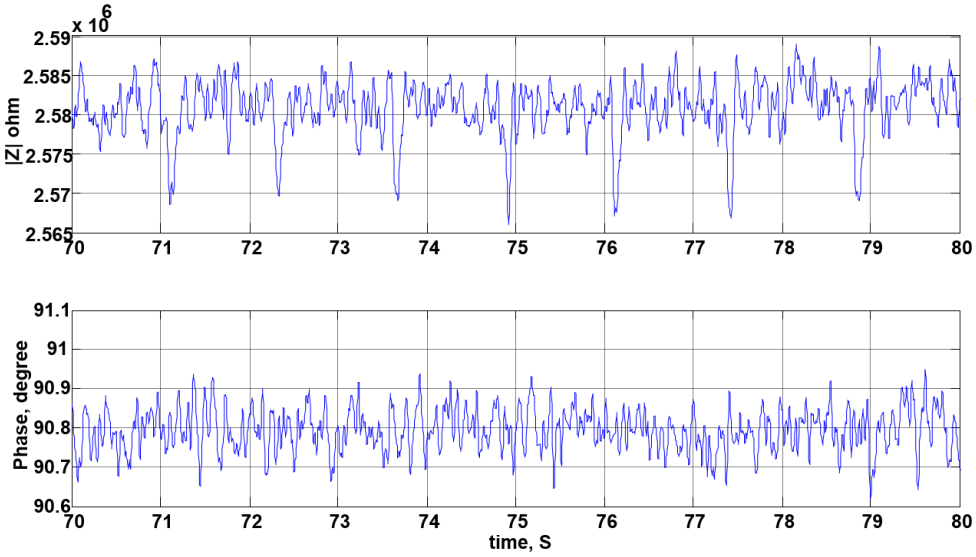

Figure 25: The differential impedance measurements (amplitude and phase) of droplets at 100 KHz.

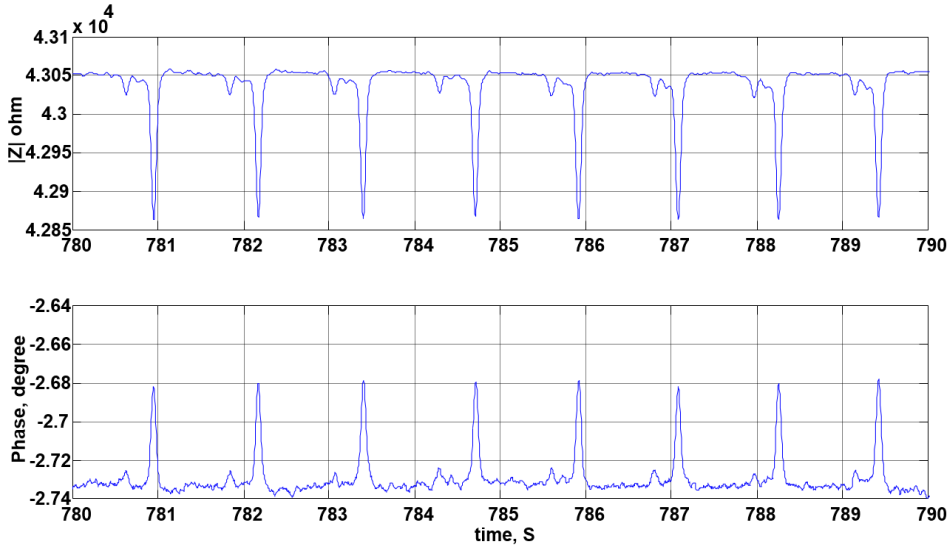

Figure 26: The differential impedance measurements (amplitude and phase) of droplets at 20 MHz.

Figure 25 and Figure 26 show the impedance measurements of both the real and phase response for droplets passing through the detection region as shown in Figure 27. The real impedance change values gradually decreased when the frequency increased. As shown in Figure 25and Figure 26, the real impedance change when the droplets of 200 μm passed between the two electrodes, negative peaks were shown after filtering out the positive peaks for further baseline analysis. From 100 KHz to 20 MHz, the real impedance value drop was $14.212X10^3$ Ω.

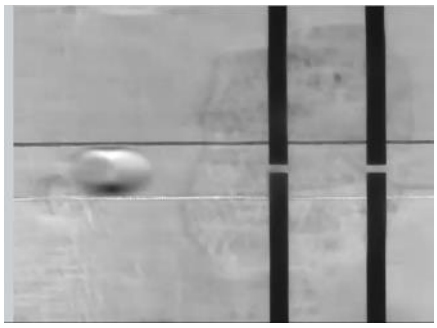

Figure 27: A droplet passing the differential electrodes.

For an overall view, Figure 28 shows how the average impedance change dropped when the frequency increased. However, Figure 29 demonstrates gradually increasing starting from 8 MHz, whereas the phase response before this frequency was non usable as shown in Figure 25.

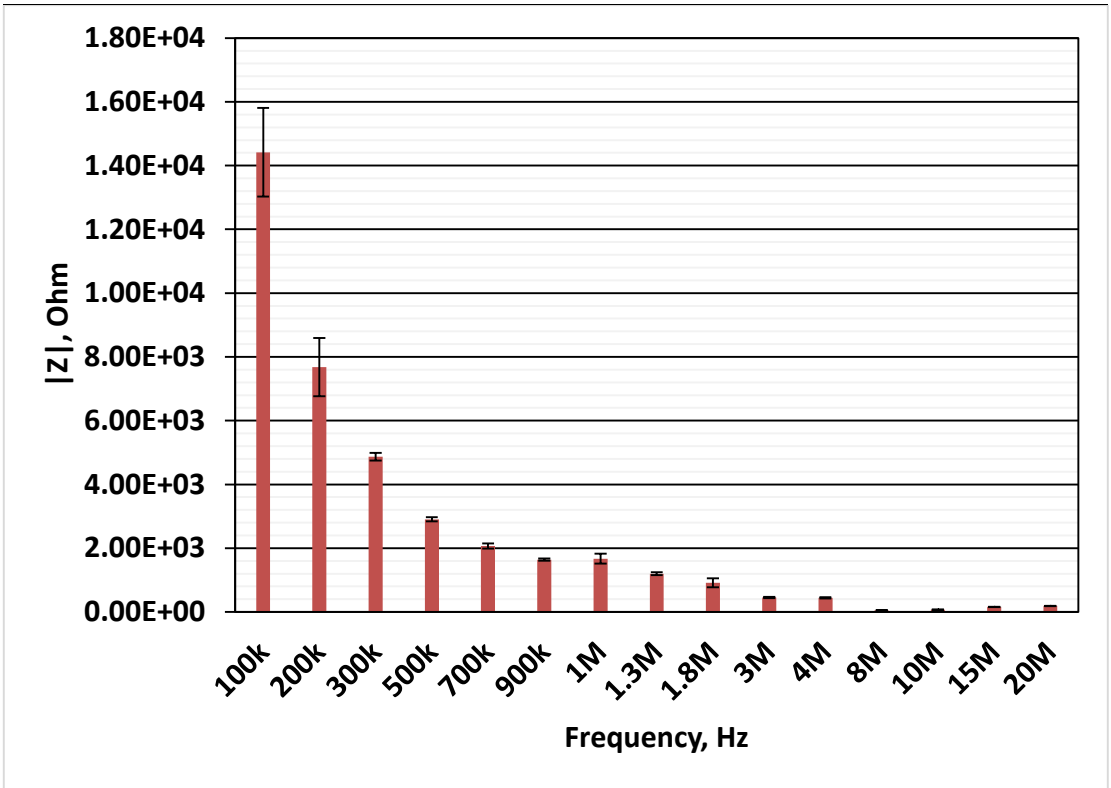

Figure 28: The amplitude impedance change of droplets passing between the differential electrodes.

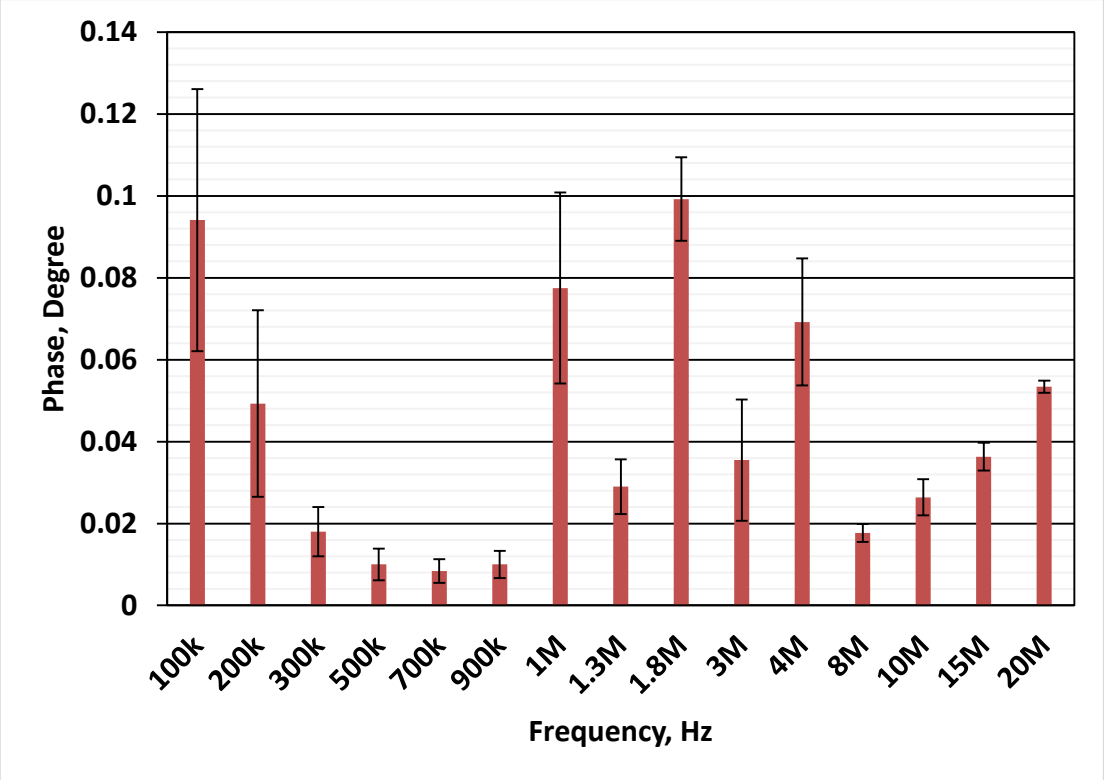

Figure 29: The phase change of droplets passing between the differential electrodes.

The mean, standard deviation, and relative standard deviation of both amplitude and phase are represented in Table 4.

Table 4: Differential impedance measurements.

	Amplitude (Ω)			Phase (Degree)		
freq (Hz)	Mean	SD	RSD (%)	Mean	SD	RSD (%)
100k	14400	1390	9.64	0.0941	0.0320	34.01
200k	7680	913	11.90	0.0493	0.0228	46.25
300k	4870	124	2.55	0.0180	0.0060	33.33
500k	2900	65.2	2.25	0.0100	0.0039	39.00
700k	2070	84.6	4.09	0.0084	0.0029	34.52
900k	1640	33	2.01	0.010	0.0033	33.00
1M	1670	154	9.21	0.0775	0.0233	30.07
1.3M	1200	44.6	3.72	0.0290	0.0067	23.10
1.8M	912	139	15.21	0.0992	0.0102	10.28
3M	457	18.9	4.13	0.0355	0.0148	41.69
4M	446	20.3	4.55	0.0692	0.0155	22.40
8M	55.1	0.78	1.41	0.0177	0.0022	12.43
10M	69.1	2.06	2.98	0.0264	0.0044	16.70
15M	160	3.54	2.21	0.0363	0.0034	9.37
20M	188	1.81	0.97	0.0534	0.0015	2.81

4.2.2. Sorting System

Based on this high-throughput detection achievement, microdroplets manipulation using sorting techniques could be combined to this novel platform for highly integrated device. Sorting of droplets-based microfluidic systems have been separately tested and succeeded using different techniques and schematics. The two sorting methods have been designed and tested: valve-based pneumatic sorting and electrical field-based sorting as shown in Figure 30 and Figure 31. This sorting system could be employed and integrated

to the impedance spectroscopy device to sort the microdroplets based on their integrated impedance measurements.

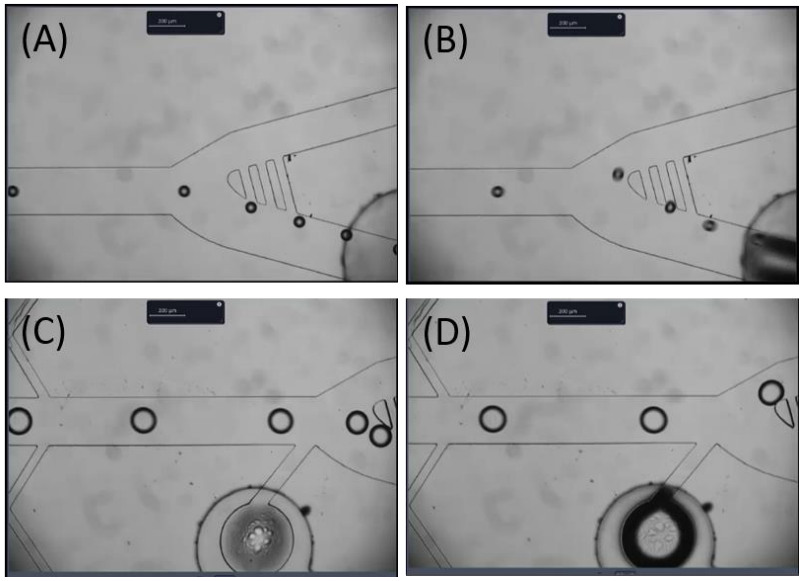

Figure 30: Four different pneumatic sorting devices. (a and b) show small size droplets in valve-based microfluidic systems where in (a) the droplets flow to the waste channel while in (b) one target droplet was deflected to the upper sorting channel. Another design was fabricated and tested using side pushing sorter as shown in (c and d).

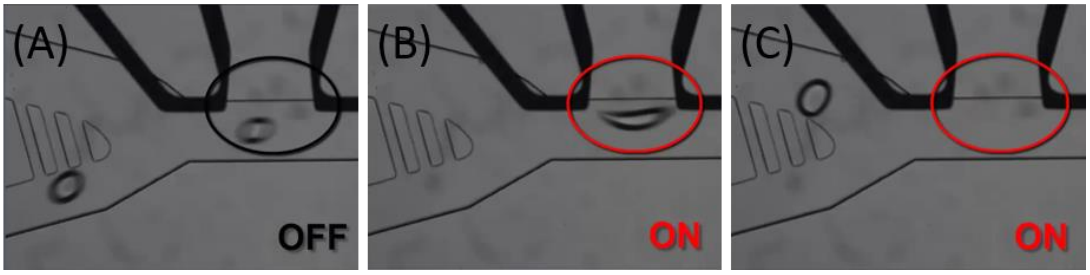

Figure 31: Electrical field based sorting system. (a) It shows the normal droplets flow without electrical field. (b) It shows that the effect of the electric field on the target droplet. (c) The target droplet defect to the sorting channel due to the applied electric field.

REFERENCES

[1] S. Y. Teh, R. Lin, L. H. Hung, and A. P. Lee, "Droplet microfluidics," *Lab Chip,* vol. 8, pp. 198-220, Feb 2008.

[2] H. Frèohlich, *Theory of dielectrics; dielectric constant and dielectric loss*. Oxford,: Clarendon Press, 1949.

[3] J. B. Hasted, *Aqueous dielectrics*. London,: Chapman and Hall Distributed in the U.S.A. by Halsted Press, a division of J. Wiley & Sons, New York, 1973.

[4] P. Cicmanec, "Cavity Perturbation Method for Measurement of Permittivity and Conductivity of Medium Lossy Semiconductors and Dielectrics," *Solid-State Electronics,* vol. 14, pp. 153-&, 1971.

[5] J. Barthel, K. Bachhuber, R. Buchner, and H. Hetzenauer, "Dielectric Spectra of Some Common Solvents in the Microwave Region - Water and Lower Alcohols," *Chemical Physics Letters,* vol. 165, pp. 369-373, Jan 19 1990.

[6] J. F. Rouleau, J. Goyette, T. K. Bose, and M. F. Frechette, "Performance of a microwave sensor for the precise measurement of water vapor in gases," *Ieee Transactions on Dielectrics and Electrical Insulation,* vol. 7, pp. 825-831, Dec 2000.

[7] S. S. Merchant, S. E. Prochnik, O. Vallon, E. H. Harris, S. J. Karpowicz, G. B. Witman, *et al.*, "The Chlamydomonas genome reveals the evolution of key animal and plant functions," *Science,* vol. 318, pp. 245-251, Oct 12 2007.

[8] S. Gawad, K. Cheung, U. Seger, A. Bertsch, and P. Renaud, "Dielectric spectroscopy in a micromachined flow cytometer: theoretical and practical considerations," *Lab on a Chip,* vol. 4, pp. 241-251, 2004.

[9] H. Morgan, T. Sun, D. Holmes, S. Gawad, and N. G. Green, "Single cell dielectric spectroscopy," *Journal of Physics D-Applied Physics,* vol. 40, pp. 61-70, Jan 7 2007.

[10] T. Sun, N. G. Green, S. Gawad, and H. Morgan, "Analytical electric field and sensitivity analysis for two microfluidic impedance cytometer designs," *Iet Nanobiotechnology,* vol. 1, pp. 69-79, Oct 2007.

[11] T. Sun, S. Gawad, C. Bernabini, N. G. Green, and H. Morgan, "Broadband single cell impedance spectroscopy using maximum length sequences: theoretical

analysis and practical considerations," *Measurement Science & Technology,* vol. 18, pp. 2859-2868, Sep 2007.

[12] T. Sun and H. Morgan, "Single-cell microfluidic impedance cytometry: a review," *Microfluidics and Nanofluidics,* vol. 8, pp. 423-443, Apr 2010.

[13] C. G. Cooney, C. Y. Chen, M. R. Emerling, A. Nadim, and J. D. Sterling, "Electrowetting droplet microfluidics on a single planar surface," *Microfluidics and Nanofluidics,* vol. 2, pp. 435-446, Sep 2006.

[14] C. Hansen and S. R. Quake, "Microfluidics in structural biology: smaller, faster... better," *Current Opinion in Structural Biology,* vol. 13, pp. 538-544, Oct 2003.

[15] P. Yager, T. Edwards, E. Fu, K. Helton, K. Nelson, M. R. Tam, *et al.*, "Microfluidic diagnostic technologies for global public health," *Nature,* vol. 442, pp. 412-418, Jul 27 2006.

[16] J. El-Ali, P. K. Sorger, and K. F. Jensen, "Cells on chips," *Nature,* vol. 442, pp. 403-411, Jul 27 2006.

[17] G. M. Whitesides, "The origins and the future of microfluidics," *Nature,* vol. 442, pp. 368-373, Jul 27 2006.

[18] E. K. Sackmann, A. L. Fulton, and D. J. Beebe, "The present and future role of microfluidics in biomedical research," *Nature,* vol. 507, pp. 181-189, Mar 13 2014.

[19] J. Friend and L. Yeo, "Fabrication of microfluidic devices using polydimethylsiloxane," *Biomicrofluidics,* vol. 4, Jun 2010.

[20] C. R. W. Tamanaha, L. J. ; Colton, R. J., "Hybrid macro–micro fluidics system for a chip-based biosensor," *Journal of Micromechanics and Microengineering,* vol. 12, 2002.

[21] K. Kim, S. Park, J. B. Lee, H. Manohara, Y. Desta, M. Murphy, *et al.*, "Rapid replication of polymeric and metallic high aspect ratio microstructures using PDMS and LIGA technology," *Microsystem Technologies,* vol. 9, pp. 5-10, Nov 2002.

[22] A. Manz, N. Graber, and H. M. Widmer, "Miniaturized Total Chemical-Analysis Systems - a Novel Concept for Chemical Sensing," *Sensors and Actuators B-Chemical,* vol. 1, pp. 244-248, Jan 1990.

[23] D. R. Reyes, D. Iossifidis, P. A. Auroux, and A. Manz, "Micro total analysis systems. 1. Introduction, theory, and technology," *Analytical Chemistry,* vol. 74, pp. 2623-2636, Jun 15 2002.

[24] C. T. Culbertson, T. G. Mickleburgh, S. A. Stewart-James, K. A. Sellens, and M. Pressnall, "Micro Total Analysis Systems: Fundamental Advances and Biological Applications," *Analytical Chemistry,* vol. 86, pp. 95-118, Jan 7 2014.

[25] L. S. Jang and M. H. Wang, "Microfluidic device for cell capture and impedance measurement," *Biomedical Microdevices,* vol. 9, pp. 737-743, Oct 2007.

[26] D. Malleo, J. T. Nevill, L. P. Lee, and H. Morgan, "Continuous differential impedance spectroscopy of single cells," *Microfluidics and Nanofluidics,* vol. 9, pp. 191-198, Aug 2010.

[27] S. Z. Hua and T. Pennell, "A microfluidic chip for real-time studies of the volume of single cells," *Lab on a Chip,* vol. 9, pp. 251-256, 2009.

[28] Y. Cho, H. S. Kim, A. B. Frazier, Z. G. Chen, D. M. Shin, and A. Han, "Whole-Cell Impedance Analysis for Highly and Poorly Metastatic Cancer Cells," *Journal of Microelectromechanical Systems,* vol. 18, pp. 808-817, Aug 2009.

[29] D. Di Carlo, L. Y. Wu, and L. P. Lee, "Dynamic single cell culture array," *Lab on a Chip,* vol. 6, pp. 1445-1449, 2006.

[30] D. Di Carlo, N. Aghdam, and L. P. Lee, "Single-cell enzyme concentrations, kinetics, and inhibition analysis using high-density hydrodynamic cell isolation arrays," *Analytical Chemistry,* vol. 78, pp. 4925-4930, Jul 15 2006.

[31] A. M. Skelley, O. Kirak, H. Suh, R. Jaenisch, and J. Voldman, "Microfluidic control of cell pairing and fusion," *Nature Methods,* vol. 6, pp. 147-152, Feb 2009.

[32] G. Benazzi, D. Holmes, T. Sun, M. C. Mowlem, and H. Morgan, "Discrimination and analysis of phytoplankton using a microfluidic cytometer," *Iet Nanobiotechnology,* vol. 1, pp. 94-101, Dec 2007.

[33] D. Holmes, D. Pettigrew, C. H. Reccius, J. D. Gwyer, C. van Berkel, J. Holloway, *et al.*, "Leukocyte analysis and differentiation using high speed microfluidic single cell impedance cytometry," *Lab on a Chip,* vol. 9, pp. 2881-2889, 2009.

[34] K. C. Cheung, M. Di Berardino, G. Schade-Kampmann, M. Hebeisen, A. Pierzchalski, J. Bocsi, *et al.*, "Microfluidic Impedance-Based Flow Cytometry," *Cytometry Part A,* vol. 77A, pp. 648-666, Jul 2010.

[35] S. Gawad, L. Schild, and P. Renaud, "Micromachined impedance spectroscopy flow cytometer for cell analysis and particle sizing," *Lab on a Chip,* vol. 1, pp. 76-82, 2001.

[36] K. Cheung, S. Gawad, and P. Renaud, "Impedance spectroscopy flow cytometry: On-chip label-free cell differentiation," *Cytometry Part A,* vol. 65A, pp. 124-132, Jun 2005.

[37] Y. F. Wu, J. D. Benson, and M. Almasri, "Micromachined Coulter counter for dynamic impedance study of time sensitive cells," *Biomedical Microdevices,* vol. 14, pp. 739-750, Aug 2012.

[38] G. Mernier, E. Duqi, and P. Renaud, "Characterization of a novel impedance cytometer design and its integration with lateral focusing by dielectrophoresis," *Lab on a Chip,* vol. 12, pp. 4344-4349, 2012.

[39] F. B. Myers, C. K. Zarins, O. J. Abilez, and L. P. Lee, "Label-free electrophysiological cytometry for stem cell-derived cardiomyocyte clusters," *Lab on a Chip,* vol. 13, pp. 220-228, 2013.

[40] G. Mernier, N. Piacentini, R. Tornay, N. Buffi, and P. Renaud, "Cell viability assessment by flow cytometry using yeast as cell model," *Sensors and Actuators B-Chemical,* vol. 154, pp. 160-163, Jun 20 2011.

[41] T. Sun, D. Holmes, S. Gawad, N. G. Green, and H. Morgan, "High speed multi-frequency impedance analysis of single particles in a microfluidic cytometer using maximum length sequences," *Lab on a Chip,* vol. 7, pp. 1034-1040, 2007.

[42] T. Lanz, S. Hafizovic, J. Rothe, R. Streichan, N. Goedecke, F. Heer, *et al.*, "Differential impedance spectrometer and vision system for analysis of single cells," in *Solid-State Sensors, Actuators and Microsystems Conference, 2009. TRANSDUCERS 2009. International*, 2009, pp. 1297-1300.

[43] N. M. Haandbæk, K.; R. Streichan; Goedecke, N. ; Bürgel, S. C. ; Heer, F.; Hierlemann, A., "Characterization of Cell Phenotype Using Dynamic Vision Sensor and Impedance Spectroscope," in *μTAS 2011*, 2011, pp. 2-6.

[44] S. C. Burgel, Z. Zhu, N. Haandbaek, O. Frey, and A. Hierlemann, "Dynamic and Static Impedance Spectroscopy for Single Particle Characterization in Microfluidic Chips," *2012 Ieee 25th International Conference on Micro Electro Mechanical Systems (Mems),* 2012.

[45] S. Emaminejad, M. Javanmard, R. W. Dutton, and R. W. Davis, "Microfluidic diagnostic tool for the developing world: contactless impedance flow cytometry," *Lab on a Chip,* vol. 12, pp. 4499-4507, 2012.

[46] K. Cheung, S. Gawad, and P. Renaud, "Microfluidic impedance spectroscopy flow cytometer: Particle size calibration," *Mems 2004: 17th Ieee International Conference on Micro Electro Mechanical Systems, Technical Digest,* pp. 343-346, 2004.

[47] N. Haandbaek, S. C. Burgel, F. Heer, and A. Hierlemann, "Characterization of subcellular morphology of single yeast cells using high frequency microfluidic impedance cytometer," *Lab on a Chip,* vol. 14, pp. 369-377, 2014.

[48] J. A. Chen, Y. Zheng, Q. Y. Tan, Y. L. Zhang, J. Li, W. R. Geddie, *et al.*, "A microfluidic device for simultaneous electrical and mechanical measurements on single cells," *Biomicrofluidics,* vol. 5, Mar 2011.

[49] J. Chen, Y. Zheng, Q. Y. Tan, E. Shojaei-Baghini, Y. L. Zhang, J. Li, *et al.*, "Classification of cell types using a microfluidic device for mechanical and electrical measurement on single cells," *Lab on a Chip,* vol. 11, pp. 3174-3181, 2011.

[50] Q. Y. Tan, G. A. Ferrier, B. K. Chen, C. Wang, and Y. Sun, "Quantification of the specific membrane capacitance of single cells using a microfluidic device and impedance spectroscopy measurement," *Biomicrofluidics,* vol. 6, Sep 2012.

[51] Y. Zhao, D. Y. Chen, Y. N. Luo, H. Li, B. Deng, S. B. Huang, *et al.*, "A microfluidic system for cell type classification based on cellular size-independent electrical properties," *Lab on a Chip,* vol. 13, pp. 2272-2277, 2013.

[52] C. Bernabini, D. Holmes, and H. Morgan, "Micro-impedance cytometry for detection and analysis of micron-sized particles and bacteria," *Lab on a Chip,* vol. 11, pp. 407-412, 2011.

[53] M. Evander, A. J. Ricco, J. Morser, G. T. A. Kovacs, L. L. K. Leung, and L. Giovangrandi, "Microfluidic impedance cytometer for platelet analysis," *Lab on a Chip,* vol. 13, pp. 722-729, 2013.

[54] A. A. S. Bhagat, S. S. Kuntaegowdanahalli, N. Kaval, C. J. Seliskar, and I. Papautsky, "Inertial microfluidics for sheath-less high-throughput flow cytometry," *Biomedical Microdevices,* vol. 12, pp. 187-195, Apr 2010.

[55] J. F. Edd, D. Di Carlo, K. J. Humphry, S. Koster, D. Irimia, D. A. Weitz, *et al.*, "Controlled encapsulation of single-cells into monodisperse picolitre drops," *Lab on a Chip,* vol. 8, pp. 1262-1264, Aug 2008.

[56] P. M. Gunther, F. Moller, T. Henkel, J. M. Kohler, and G. A. Gross, "Formation of monomeric and novolak azo dyes in nanofluid segments by use of a double injector chip reactor," *Chemical Engineering & Technology,* vol. 28, pp. 520-527, Apr 2005.

[57] D. K. Hwang, D. Dendukuri, and P. S. Doyle, "Microfluidic-based synthesis of non-spherical magnetic hydrogel microparticles," *Lab on a Chip,* vol. 8, pp. 1640-1647, Oct 2008.

[58] I. Shestopalov, J. D. Tice, and R. F. Ismagilov, "Multi-step synthesis of nanoparticles performed on millisecond time scale in a microfluidic droplet-based system," *Lab on a Chip,* vol. 4, pp. 316-321, 2004.

[59] J. Q. Boedicker, L. Li, T. R. Kline, and R. F. Ismagilov, "Detecting bacteria and determining their susceptibility to antibiotics by stochastic confinement in nanoliter droplets using plug-based microfluidics," *Lab on a Chip,* vol. 8, pp. 1265-1272, Aug 2008.

[60] E. Brouzes, M. Medkova, N. Savenelli, D. Marran, M. Twardowski, J. B. Hutchison, *et al.*, "Droplet microfluidic technology for single-cell high-throughput screening," *Proceedings of the National Academy of Sciences of the United States of America,* vol. 106, pp. 14195-14200, Aug 25 2009.

[61] J. Clausell-Tormos, D. Lieber, J. C. Baret, A. El-Harrak, O. J. Miller, L. Frenz, *et al.*, "Droplet-based microfluidic platforms for the encapsulation and screening of mammalian cells and multicellular organisms," *Chemistry & Biology,* vol. 15, pp. 427-437, May 2008.

[62] H. Song, D. L. Chen, and R. F. Ismagilov, "Reactions in droplets in microflulidic channels," *Angewandte Chemie-International Edition,* vol. 45, pp. 7336-7356, 2006.

[63] S. Koster, F. E. Angile, H. Duan, J. J. Agresti, A. Wintner, C. Schmitz, *et al.*, "Drop-based microfluidic devices for encapsulation of single cells," *Lab on a Chip,* vol. 8, pp. 1110-1115, 2008.

[64] E. Um, S. G. Lee, and J. K. Park, "Random breakup of microdroplets for single-cell encapsulation," *Applied Physics Letters,* vol. 97, Oct 11 2010.

[65] A. Weltin, K. Slotwinski, J. Kieninger, I. Moser, G. Jobst, M. Wego, *et al.*, "Cell culture monitoring for drug screening and cancer research: a transparent,

microfluidic, multi-sensor microsystem," *Lab on a Chip,* vol. 14, pp. 138-146, 2014.

[66] E. W. M. Kemna, L. I. Segerink, F. Wolbers, I. Vermes, and A. van den Berg, "Label-free, high-throughput, electrical detection of cells in droplets," *Analyst,* vol. 138, pp. 4585-4592, 2013.

[67] Y. N. Xia and G. M. Whitesides, "Soft lithography," *Angewandte Chemie-International Edition,* vol. 37, pp. 551-575, Mar 16 1998.

[68] Z. Instrumnets, "HF2 User Manual," 23220 ed, Apr. 2014.

[69] E. H. Harris, *The Chlamydomonas sourcebook: introduction to Chlamydomonas and its laboratory use* vol. 1: Academic Press, 2009.

[70] H. J. Lee, J. H. Lee, H. S. Moon, I. S. Jang, J. S. Choi, J. G. Yook, *et al.*, "A planar split-ring resonator-based microwave biosensor for label-free detection of biomolecules," *Sensors and Actuators B-Chemical,* vol. 169, pp. 26-31, Jul 5 2012.

APPENDIX A

MASK DESIGN

MASK DESIGN: MICROFLUIDIC LAYER

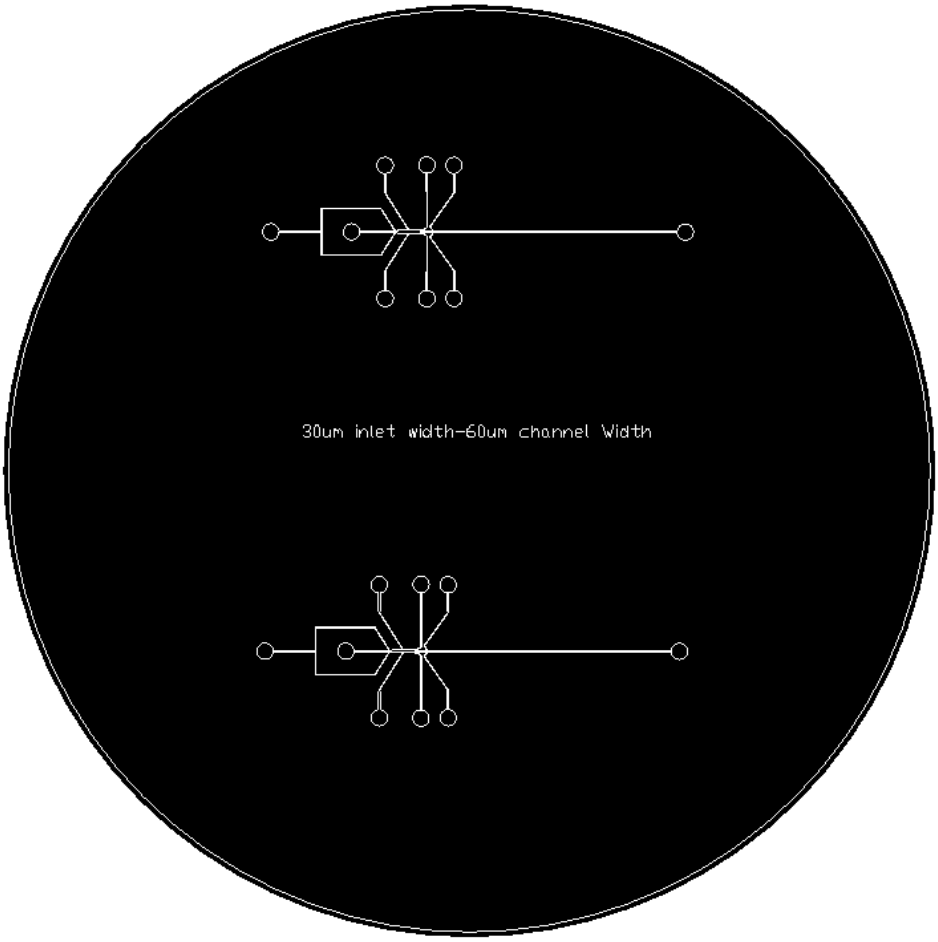

Figure A.1: Mask film of the droplet –based microfluidic impedance spectroscopy device.

MASK DESIGN: MICROELECTRODES PATTEREN

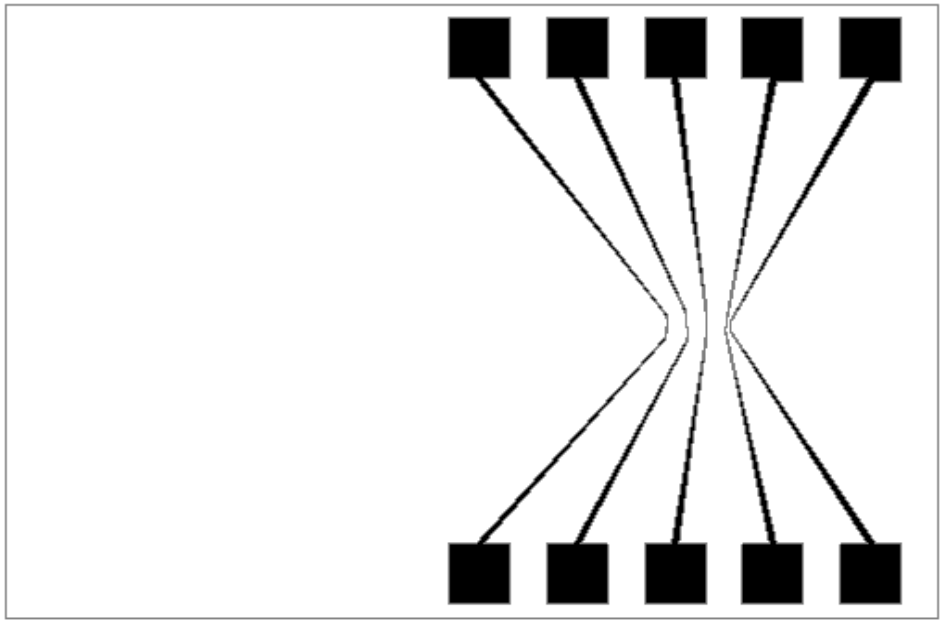

Figure A.2: Mask layout of 5 pairs of microelectrodes.

APPENDIX B

MASTER FABRICATION PROCEDURE

B.1. Microfluidic Channel Layer Master Fabrication Procedure

1. Clean a 3 inch wafer by rinsing using acetone, IPA, methanol, DI water, and drying with nitrogen (N_2) gas
2. Remove remaining solvents by baking at 200ºC for 10 minutes
3. Spin coated at two different speed using negative photoresist (SU-8 2050), 500 rpm for 10 s to uniform the photoresist on the wafer, then 2900 rpm for 30 s to exactly yield 60 µm photoresist thickness.
4. soft baking using a hotplate for 12 hr at 65 ºC and 40 min at 95 ºC.
5. Expose the wafer to UV light (Karl Suss MA6 Mask Aligner) using dark field mask at dosage of 200 mJ/cm^2
6. Hard baking the wafers at 65 ºC for 40min and 95 ºC for 20min.
7. Develop the wafer using Thinner type P to remove the non-exposed photoresist by immersing the wafer inside the developer until the non-exposed photoresist completely removed
8. Rinse the wafer with IPA and dried with N_2 gas

B.2. Microelectrodes Pattern Fabrication Procedure

1. Clean 2 x 3 inch glass slides glass slides using the piranha cleaning process.

2. Deposit a uniform of (Au/Ti) layer using E-beam evaporation equipment (Lesker PVD 75 Ebeam Evaporator) of thickness 2000/200Å.
3. Spin coat a positive photoresist, S1818 at 3000 rpm for 30 s onto a gold coated slide
4. Soft bake the glass slides at 95 ºC for 10min
5. Expose the glass slide to UV light (Karl Suss MA6 Mask Aligner) using clearfiled pattern mask to perform the electrode pattern at 85 mJ/cm^2
6. Hard bake the glass slides at 110 ºC for 2 min
7. Develop the slides for 30 s using MF319 to remove the exposed area
8. Immerse the patterned slides in Au etchant (Type TFA, Transene Company Inc.) to remove the exposed area
9. Etch the exposed Ti area using Ti etchant (HF:H2O at 1:300).
10. Remove the remaining photoresist using acetone.
11. Clean the pattern gold electrodes using DI water and dry by N_2 gas.

APPENDIX C

PDMS DEVICE FABRICATION PROCEDURE

C.1. PDMS Passivation layer on Microelectrodes Fabrication Procedure

1. Mix 3 gram of PDMS prepolymer (Sylgrad 184, Dow Corning, Inc) with the curing agent at 10:1 ratio
2. Degas the PPDMS mixture using desiccator for 15 min
3. Mix the PDMS mixture with hexane at ratio (1:1)
4. Pour 4 gram of the mixture on the patterened gold glass slide
5. Spin coat at 4000 rpm for 1 min
6. Place the coated slide in oven for curing at 85ºC for 6 hr

C.2. Microfluidic PDMS Layer Fabrication Procedure

1. Coat the fabricated microfluidic master wafer with tridecafluoro-1,1,2,2-tetrahydroocty-l,1,2,2- tetrahydrooctyl (trichlorosilane, United Chemical Technologies, Inc.) by placing the fabricated wafer inside the desiccator chamber together with 6 ~ 7 drops of trichlorosilane in weight boats
2. Degas the desiccator chamber for 20 min to vaporize the trichlorosilane and coat the fabricated pattern wafer
3. Clean the coated patterned wafer with Isopropyl alcohol (IPA) and dry with N_2 gas
4. Mix 20 gram of PDMS prepolymer (Sylgrad 184, Dow Corning, Inc) with the curing agent at 10:1 ratio

5. Degas the PDMS mixture using the desiccator for 15 min
6. Place and fix the coated patterned wafer in petri dish using tape
7. Pour the PDMS mixture on the coated patterned wafer
8. Place the petri dish inside the desiccator chamber and degas for 15 min
9. Cure at 85ºC for 2 hr

C.3. Microfluidic PDMS Methanol Boning Procedure

1. Peel off the cured PDMS microfluidic channel layer
2. Punch the inlets and outlets using a needle of gauge 19
3. Place the PDMS microfluidic channel layer and coated gold electrodes glass slide inside the oxygen plasma treatment (100mTorr and 100 W) for 1.5 min
4. Rinse the coated gold electrodes glass slide with methanol
5. Align the microfluidic layer on the coated electrodes
6. Bake assembled device at 80 ºC for 8 hr

APPENDIX D

IMPEDANCE ANALYZER EXPERIMENTAL PROCEDURE

D.1. Experimental Set-UP Procedure

1. Solder 2 SMA connectors (CONN SMA JACK STR 50 OHM PCB, J494-ND, ROHS COMP) on the patterned gold pads after removing the coated PDMS from these pads
2. Place the fabricated device on Zeiss microscope (Zeiss 200M inverted microscope using a HAMAMATSU Digital CMOS Camera ORCA-Flah2.8 C11440, Carl Zeiss).
3. Connect the SMA/BNC cable (CABLE SMA/BNC 6" RG-316, J3606-ND, ROHS COMP) to the input soldered SMA connector
4. Connect the SMA/SMA cable (CABLE SMA/SMA 6" RG-316, J3706-ND, ROHS COMP) to the output soldered SMA connector
5. Connect the another end of the SMA/SMA cable to the current amplifier (HF2TA Current Amplifier, Zurich Instruments AG)
6. Connect the BNC of the SMA/BNC cable to the impedance analyzer (HF2IS Impedance Spectroscopy, Zurich Instruments AG)
7. Connect the current amplifier to the impedance analyzer (ZCtrl connector) using a standard straight-through as opposed to cross-over of single Ethernet cable to power and control signals.
8. Connect the impedance analyzer to the PC using USB cable
9. Power on the impedance analyzer and Zeiss microscope

D.2. Experimental Procedure

1. Start the ziControl software

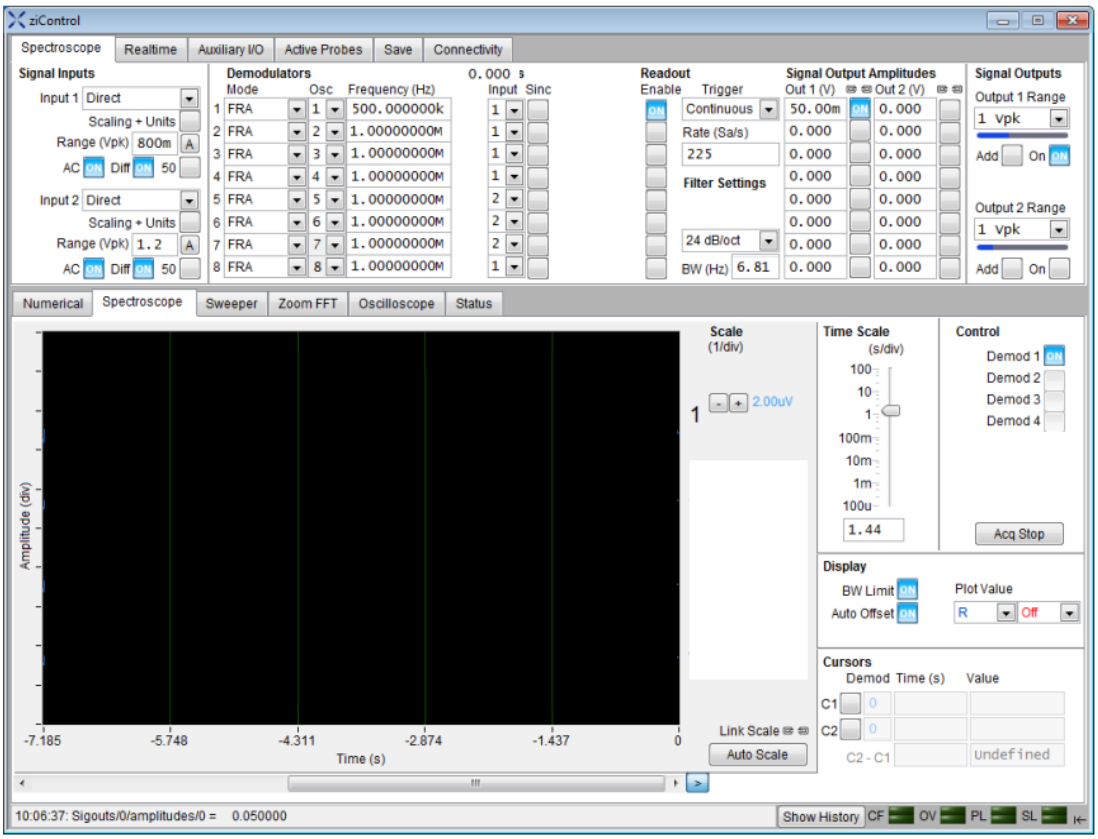

Figure D.1: ziControl impedance spectroscopy interface

2. Set the signal output amplitude to 1 Volt
3. Set the sampling rate to 1.8 KS/s
4. Select the 8th filter order
5. Enable the first readout
6. Select 2-Term Z in Mode Demodulators section
7. Set the excitation frequency to 550 KHz

8. From the Input Signal section, select the input 1 of the HF2TA current amplifier
9. Disable the Diff button
10. Enable the AC button
11. Enable the On button from the Signal Input section
12. Press the A button of the range
13. From the bottom menu of the interface, enable the Demo 1 under the Spectroscope tab